

Exploring the morphological development of embryo dunes in Terschelling using unmanned aerial vehicle imagery

Bram Schipper



© Photo: Gerrit-Bart Volgers



WAGENINGEN
UNIVERSITY & RESEARCH

Exploring the morphological development of embryo dunes in Terschelling using unmanned aerial vehicle imagery

Bram Schipper

Registration number 190419739090

Supervisors:

dr.ir. Lammert Kooistra

dr. Juul Limpens

A thesis submitted in partial fulfilment of the degree of Master of Science
at Wageningen University and Research Centre, the Netherlands.

October 2018

Wageningen, the Netherlands

Thesis code number: GRS-80436

Thesis Report: GIRS-2018-50

Wageningen University and Research Centre

Laboratory of Geo-Information Science and Remote Sensing

Abstract

Dunes act as a flexible natural flood defence and protect low-lying areas from flooding by the sea. Due to climate change more and more man-made measures such as sand nourishments are needed to counteract coastal erosion and maintain safety of the inland. However, these measures are not always the best solution from a financial and environmental perspective. Adaptive measures like building with nature concepts can possibly help maintain and develop the coast by for example stimulating new dune formations.

Natural dune development in coastal zones is the result of an interaction between vegetation and different dynamic processes influencing sedimentation and erosion. A lot of research has been done on processes and factors influencing sand supply to the dunes. However, how the development of embryo dunes is influenced by different spatial factors and dune characteristics and its relative individual impact is less known.

This study explored how geomorphological development of embryo dunes can be monitored by using imagery acquired from unmanned aerial vehicles (UAV) and analysed the main drivers influencing this development. An experimental dune field called 'Windwerk' located on the Wadden island Terschelling in the Netherlands was monitored between May 2016 and June 2017 with six observations from a UAV equipped with a digital camera system. Windwerk consist of 32 unique dune fields where embryo dunes (young dune formations) are naturally created by planting grasses on the beach with all a different amount of vegetation and spatial design. This makes the Windwerk experiment an excellent opportunity to study different aspects and causal relations of different main drivers that are influencing early dune development.

For every dataset a digital surface model (DSM) and orthomosaic was reconstructed with a 0.05m resolution by applying a structure from motion method. From this DSM, a digital terrain model (DTM) was derived where after a dune model was extracted by using a slope-based filtering technique. Based on the final dune models, different explanatory factors were related to changes between the dune fields over summer, winter and a full year.

The applied method of this study was very useful for reconstructing 3D dune models from aerial UAV imagery to quantify dune volume/size changes over time. The results indicate that short-term changes are mainly expressed by the temporal sand shadows behind vegetation, whereas long-term development is expressed by accumulation of sand in between individual neighbouring dunes. During one year an overall positive change in dune volume can be found for most dune fields. However, some exposed dune fields on the edge of the study area did not develop. Summer development was mainly determined by the amount of planted grass plots and sheltering by other fields, whereas winter development was influenced by the beach elevation and terrain roughness. The applied methodology of this study can be used in comparable studies using UAV's to monitor dunes and morphological development. The results of this study can be valuable for coastal management strategies and can support future decision making in the design and implementation of vegetation as a tool for adaptive coastal defences.

Keywords: *Unmanned Aerial Vehicle (UAV), Structure from Motion, DTM extraction, embryo dune, embryo dune development, geomorphology, Windwerk, building with nature*

Table of Contents

ABSTRACT	IV
TABLE OF CONTENTS	V
LIST OF FIGURES	VII
LIST OF TABLES	VII
1 INTRODUCTION AND OBJECTIVES	1
1.1 BACKGROUND	1
1.2 PROBLEM DEFINITION	1
1.3 OBJECTIVE AND RESEARCH QUESTIONS	3
2 METHODS	5
2.1 STUDY AREA.....	5
2.2 DATA COLLECTION.....	6
2.3 DATA PROCESSING WORKFLOW.....	8
2.3.1 Pre-processing	9
2.3.2 DSM generation.....	9
2.3.3 DTM generation and removing artefacts	11
2.3.4 Accuracy of DSM and DTM.....	12
2.3.5 Defining dunes.....	12
2.4 DUNE DEVELOPMENT ANALYSIS.....	12
2.4.1 Dune development indicators.....	12
2.4.2 Dune development over time	13
2.4.3 Explanatory variables	13
2.4.4 Statistical analysis	15
3 RESULTS	16
3.1 QUANTIFYING EMBRYO DUNES FROM UAV IMAGERY	16
3.1.1 DSM from structure from motion	16
3.1.2 DTM creation from DSM.....	18
3.1.3 Creating dune height model	20
3.2 DUNE DEVELOPMENT.....	21
3.2.1 Weather conditions	21
3.2.2 Changes in (embryo)dunes over time	21
3.2.3 Statistical analyses	24
4 DISCUSSION	27
4.1 CREATION OF THE DSM BY SFM.....	27
4.2 CREATION OF THE DIGITAL TERRAIN MODELS.....	27
4.3 CREATION OF DUNE HEIGHT MODEL.....	28
4.4 DUNE DEVELOPMENT OVER TIME	28
4.5 BROADER IMPLICATIONS.....	29
5 CONCLUSIONS AND RECOMMENDATIONS	31
6 REFERENCES	32
APPENDICES	35
APPENDIX A - WEATHER CONDITIONS AROUND CAMPAIGNS	36
APPENDIX B - USED SETTINGS IN AGISOFT PHOTOSCAN PRO 1.4.....	37
APPENDIX C - DIGITAL SURFACE MODELS	39

APPENDIX D	- CROSS SECTIONS DSM.....	42
APPENDIX E	– DUNE HEIGHT MODELS	43
APPENDIX F	– OVERVIEW INDIVIDUAL STUDIED FIELDS.....	46
APPENDIX G	– USED SAGA GIS TOOLS AND SOFTWARE SETTINGS.....	47

List of Figures

FIGURE 1 TYPICAL TRANSECT ACROSS SAND DUNES SHOWING DIFFERENT STAGES OF SUCCESSION (JACKSON, 2014).....	2
FIGURE 2 LOCATION OF WINDWERK SITE ON THE BEACH OF TERSCHELLING IN THE NETHERLANDS.	5
FIGURE 3 EXPERIMENTAL DESIGN OF WINDWERK SHOWING ALL 32 UNIQUE FIELDS.....	6
FIGURE 4 EXAMPLE OF A MARRAM GRASS PLOT (4M ²).....	6
FIGURE 5 TIMELINE OF THE SIX DATA ACQUISITION CAMPAIGNS CARRIED OUT WITH MUMSY SENSOR SYSTEM.....	6
FIGURE 6 FLIGHT PATHS FOR DATA COLLECTION VISUALIZED WITH GCP LOCATIONS.....	7
FIGURE 7 IMAGE OF FIXED ELEVATED REFERENCING MARKER WITHIN THE STUDY AREA.....	7
FIGURE 8 CONCEPTUAL MODEL OF DATA PROCESSING WORKFLOW AND RESEARCH STEPS.....	8
FIGURE 9 GENERATION PROCESS OF DSM MASKING LAYER.	11
FIGURE 10 30-YEAR AVERAGE WIND ROSE OF WEATHER STATION OF AMELAND (NL) - KNMI	13
FIGURE 11 POSITION INDEX CODES WITH 1) DISTANCE TO SEA, 2) DISTANCE TO EDGES, AND 3) DIAGONAL DISTANCE.....	14
FIGURE 12 DIGITAL SURFACE MODEL CREATED BY STRUCTURE-FROM-MOTION..	16
FIGURE 13 CROSS SECTIONS OF DUNE FIELD (FIELD NUMBER 23 – APPENDIX F) OF MAY 2016 (ORANGE) AND NOVEMBER 2016 (BLUE) SHOWING ELEVATION DIFFERENCES ESPECIALLY IN BETWEEN THE INDIVIDUAL DUNES.	17
FIGURE 14 DSM FROM NOVEMBER 11 (2016) SHOWING ARTEFACTS BEHIND CAUSED BY SHADOW AREAS BEHIND DUNES	18
FIGURE 15 LEFT) ENDOVI IMAGE OF DUNE COMPARED IN TIME; RIGHT) CROSS-SECTIONS OF THE SAME DUNE ON DIFFERENT MOMENTS SHOWING DIFFERENCES BETWEEN DSM AND DTM.....	18
FIGURE 16 ELEVATION DIFFERENCES BETWEEN DTM OF JUNE 2017 AND RTK HEIGHT MEASUREMENTS ACQUIRED ON OCTOBER, 27 TH 2017.....	19
FIGURE 17 CROSS-SECTION SHOWING DIFFERENCES BETWEEN DTM AND DHM.	20
FIGURE 18 DUNE MODEL OF MAY 2016 VISUALIZED (IN BLACK) ON TOP OF THE BEACH BASE PLANE	20
FIGURE 19 DUNE CHANGES BETWEEN MAY 2016 (RED) AND AUGUST 2016 (BLUE)	21
FIGURE 20 BOXPLOTS OF DUNE AREA (LEFT) AND DUNE VOLUME (RIGHT) OVER TIME.	22
FIGURE 21 BOXPLOT OF RELATIVE DUNE VOLUME CHANGES (M ³ /M ³ /WEEK).....	23
FIGURE 22 LEFT: BAR GRAPHS OF TOTAL DUNE VOLUME CHANGES [M ³] PER INDIVIDUAL FIELD. RIGHT: BAR GRAPHS OF RELATIVE DUNE VOLUME CHANGES [M ³ /M ³ /WEEK]	23
FIGURE 23 SCATTERPLOTS OF RESPONSE VARIABLE TO PREDICTOR VARIABLES OF THE PERIOD SPRING-AUTUMN 2016.....	25
FIGURE 24 SCATTERPLOT OF RESPONSE VARIABLE OF THE WINTER PERIOD TO EXPLANATORY VARIABLES OF NOVEMBER 2016.....	25
FIGURE 25 SCATTERPLOT OF RESPONSE VARIABLE OF THE FULL-YEAR DEVELOPMENT TO EXPLANATORY VARIABLES OF MAY 2016	26

List of Tables

TABLE 1 FINAL AVERAGE GCP ERROR [M] FOR EVERY DATASET SHOWING A RELATIVE HIGH ERROR FOR JUNE 2016. THE COLOUR INTENSITY CORRESPONDS TO THE MAGNITUDE OF THE AVERAGE GCP ERRORS	10
TABLE 2 MULTIPLE REGRESSION ANALYSIS FOR RELATIVE DUNE VOLUME CHANGES [M ³ /M ³ /WEEK]. THE PREDICTOR VALUES WERE TAKEN FROM EVERY FIRST DATASET OF THE STUDIED PERIOD.....	24

1 Introduction and objectives

1.1 Background

The Netherlands is a low-lying country of which the major part is located around or below sea level and therefore has to be protected from flooding by the sea. While the Dutch are well-known for their large hydrologic engineering structures which protect them against the sea, only 15 percent of the Dutch coast consist of man-made sea barriers and over 75 percent consist of natural dune areas (Koningsveld, Otten, & Mulder, 2007). Mainly because approximately 40% of the country is situated below sea level, the Netherlands is considered to be sensitive to climate change (Beniston et al., 2007). The sandy coasts are prone to erosion which are influenced by many factors such as currents, sea level, wind, and waves. All these factors are impacted by climate change and have a positive effect on coastal erosion (Saito, 2013).

Since the eighteenth-century coastal erosion control was necessary in order to stop erosion and protect the Netherlands against floods (Verhagen, 1990). Current safety standards in Dutch coastal policy are driven by the 1953 storm surge disaster, meaning that a dune is considered to be safe if it will not breach during a storm with a probability of 1:10.000 (de Winter & Ruessink, 2017). In order to maintain this requirement, man-made measures like sand nourishments are necessary to counteract the constant eroding coastline (Roggema, 2009).

Worldwide 24% of the sandy beaches are eroding with more than 0.5m/year (Luijendijk et al., 2018). According to the Intergovernmental Panel on Climate Change (IPCC), climate change adaption measures like artificially rebuilding beaches and dunes will become increasingly more difficult and expensive (Saito, 2013). Man-made measures such as sand nourishments are not always the best solution from a financial and environmental perspective.

Therefore, a new proactive approach has been embraced in order to maintain and develop the coast, called 'building with nature' (de Vriend, van Koningsveld, & Aarninkhof 2014). The idea of building with nature is to make use of natural materials, processes and dynamics which are also more adaptive to changing conditions caused by climate change (de Vriend, van Koningsveld, & Aarninkhof, 2014). In order to apply building with nature concepts to coastal protection, good insight is needed in natural processes and the development of natural dunes. Nowadays, in some cases (e.g. the Netherlands) dunes are naturally protected and stabilised by planting marram grass to trap and hold the sand within the dunes. The positive effect of vegetation to erosion protection of sandy dunes is well known, well studied and is a proven method for dune stabilisation. However, if vegetation can also be used to effectively create and develop new dune formations for coastal protection and how this can be done is less known.

1.2 Problem definition

Embryo dune development

The natural development of dunes is caused by an interaction between aeolian processes, beach morphology, vegetation and obstacles, waves and currents (Bakker et al., 2017; Carter, 1991; Hesp, 2002; Kidwell et al., 2016; Maun, 2009). Vegetation forms an obstacle and produce a reduction in wind speed within and in the lee side of the vegetation (Arnott, 2009). This facilitates deposition of sand within and around the vegetation, forming small dunes. These small dunes are also known as embryo dunes (first stage dunes). Embryo dunes are small dunes which can (temporally) trap sand and can later evolve into larger fore dunes (Van Puijenbroek et al., 2017: Figure 1).

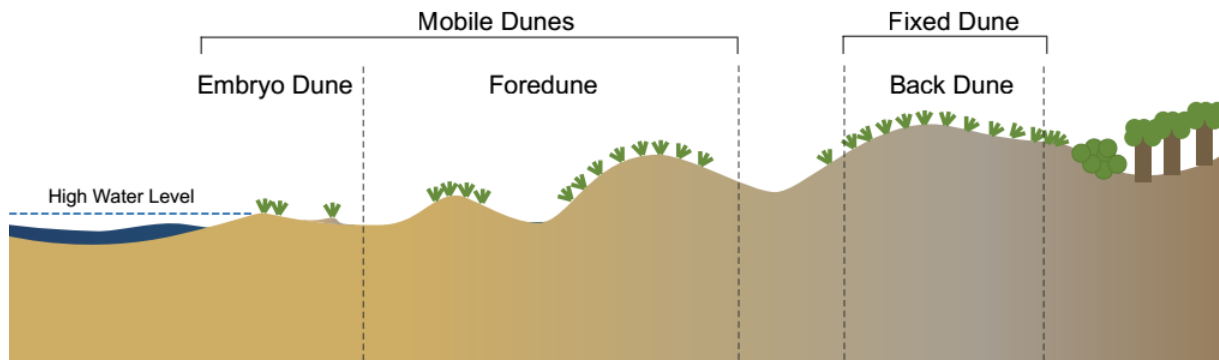


Figure 1 Typical transect across sand dunes showing different stages of succession (Jackson, 2014)

Non-vegetated embryo dunes can form by sediment transport by wind but will disappear when the wind direction changes (Maun, 2009). However, with the occurrence of vegetation, wind-blown sand will become trapped and forms an embryo dune which are more resistant to erosion and wind-direction changes. The development rate of embryo dunes is related to vegetation growth (Keijsers, De Groot, & Riksen, 2015) and is the key component to the development of embryo dunes and the development into foredunes (Arnott, 2009; Montreuil et al., 2013).

Quite some research has been done on coastal dune development focusing on factors and processes that are influencing beach morphology and sand supply (Cohn, 2018; De Vries et al., 2012; Keijsers et al., 2015; Lynch, Jackson, & Cooper, 2016; Maun, 2009; Montreuil et al., 2013; Sigren et al., 2014). However, most studies are largely restricted to descriptive monitoring work and small-scale (planting) experiments. How the development of embryo dunes is influenced by different spatial and dune characteristics is less known. Although some characteristics (e.g. dune size, vegetation) are known to be important for embryo dune development, the relative individual impact of these factors and spatio-temporal differences over time in a natural system are not known.

Monitoring

Monitoring (embryo) dune development can be done by different conventional field measurements like land surveying, which is labour-intensive, time-consuming and often spatially restricted. When monitoring large-scale dune development (e.g. volume changes), remote sensing data and derived products could play a critical role in the evaluation of spatially and temporally processes (Masek et al., 2015). With the increasing availability of remote sensing techniques and high-resolution UAV imagery, monitoring natural systems offers new possibilities for studying land-surface processes like embryo dune development. UAV (colour) imagery offers big advantages over other monitoring methods, such as land surveying which is labor-intensive, time-consuming and less accurate on large scale. Structure from motion (SfM) photogrammetry techniques can be used to process high-resolution UAV imagery (two-dimensional) into a three-dimensional digital elevation model (DEM; Mancini et al., 2013). These elevation models can be used to accurately monitor large-scale development and volume/size changes of embryo dunes by comparing elevation models over time. Alternatively, terrestrial laser scanners like LIDAR (light detection and ranging) can be used to accurately reconstruct a 3D surface. However, LIDAR systems are very expensive compared to UAV imagery and also the acquisition speed is significant lower than image-based techniques (Chandler & Buckley, 2016).

Study area

A recent 'building with nature' project is the 'Windwerk' dune experiment on the Dutch Wadden island Terschelling, where embryo dunes are naturally created by planting grasses on the beach. Different unique dune fields are created with all a different amount of vegetation and spatial design. This makes the Windwerk experiment an excellent opportunity to study different aspects and causal relations of different main drivers that are influencing early dune development, like a different size and density of dunes and vegetation in a large natural system. Normally this wouldn't be possible in a natural system since many processes coincide. Extensively monitoring the Windwerk project can potentially reveal new insights in embryo dune development which can be useful to further improve natural defenses by stimulating new dune formations. A recent and comparable study to this study has been done on the Dutch island Texel, where the contribution of vegetation and dune size to dune development was researched by using a UAV (Van Puijenbroek et al., 2017). This however was done in a natural existing dune field where individual factors are difficult to study independently.

Since the establishment of Windwerk (early 2016), an Unmanned Aerial Vehicle (UAV) equipped with a colour and near-infrared camera has been used in order to monitor the development of the vegetation and embryo dunes during different seasons. Different software packages can be used to create a digital model from UAV imagery. With the right photography strategy and data processing, SfM should rival or exceed the accuracy of laser technologies such as LIDAR (Peterson, Klein, & Stewart, 2015). The main disadvantage of SfM is that the terrain surface is often not visible when vegetation is present. In case of vegetation, the elevation of the vegetation will be measured (digital surface model) while the surface of the ground (terrain) is desired when monitoring dune development. Different filtering and interpolation techniques can be used to derive an accurate digital terrain model from the surface models. It is therefore important that the most suitable processing approach is used in order to do research on the development of small embryo dunes and studying the main drivers influencing this development.

1.3 Objective and research questions

The aim of this thesis research is to explore the morphological development of the embryo dunes of Windwerk by using UAV imagery, and find causal relations between the dune development and different explanatory factors. Also, the exact methodology to analyze dune development in space and time for this specific case and location (dune monitoring with RGB-NIR imagery) need to be studied.

The objectives of this study are: 1) find the most suitable approach for monitoring embryo dune development using UAV imagery; 2) analyze the morphological dynamics of embryo dunes and its underlying drivers.

The research questions to answer the objectives are:

- 1) What is the most suitable method for estimating a digital terrain model (DTM) of dunes with small vegetation using UAV imagery?
- 2) How accurate can a DTM be derived from a digital surface model (DSM) created by UAV photogrammetry for a sequence of different observations?
- 3) How can embryo dune development be recognized and analysed in time based on different DTM's?
- 4) How do the embryo dunes of the 'Windwerk' project develop in time looking at seasonal changes?

5) Which explanatory factors can be related to the growth rate and erosion resistance of embryo dunes?

2 Methods

In this describes the used methodology which is used to answer the research objectives. Section 2.1 first describes the study area and experimental setup of Windwerk. Section 2.2 describes the used equipment, data and data acquisition campaigns. In Section 2.3 the data processing methodology is explained which belongs to the first objective. Section 2.4 describes the dune development methodology which belongs to the second objective.

2.1 Study area

In May 2016 the experimental landscape installation 'Windwerk' was built on the beach of Terschelling, an island of the Dutch Wadden Sea (coordinates: 53° 24' 30.585" N, 5° 17' 31.9452" E), Figure 2.



Figure 2 Location of Windwerk site on the beach of Terschelling in the Netherlands.

In this experiment, new insights into embryo dune development can be explored. Windwerk is an area of 400 by 150 meters and located on the north coast of Terschelling where wind and waves have a big influence on the coast. This project was mainly set up by landscape architects on behalf of the cultural and social event 'Oerol festival' that takes place every summer on Terschelling. However, this project was also of interest to researchers from the Wageningen University because it offers various opportunities for studies in natural coastal protection. Understanding what factors and processes are influencing embryo dune development is of big interest to estimate whether natural coastal protection can help to protect sandy coasts to future rising sea levels. That's why in collaboration between the landscape architects and researchers from the Wageningen University a design has been developed that meets various interests.

Experimental design

Windwerk is a temporal art installation and 'building with nature' landscape experiment, inspired by the geometric drawings of the artist M.C. Escher. In Figure 3 the experimental design of Windwerk is visualised. The Windwerk experimental site is divided into 32 unique fields with a varying amount of vegetated plots and unique spatial design (Doedens et al., 2017: Figure 3). This is done in order to make

the area visual appealing to visitors of Terschelling, but also to explore different individual aspects that are influencing vegetation and dune development in a natural system.

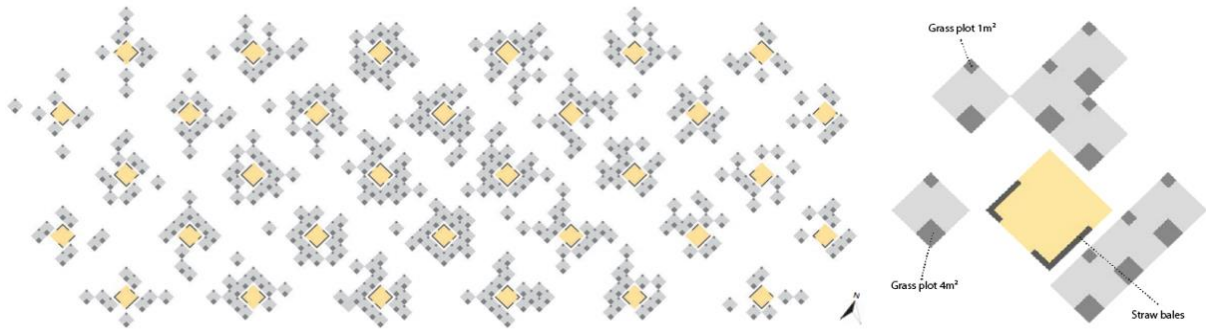


Figure 3 Experimental design of Windwerk showing all 32 unique fields with in the middle of each field an open area (yellow squares) surrounded with straw bales. Each field consist of a varying amount of subplots (gray squares) which area randomly arranged within the fields. Each subplot contains a 1 m² and 4m² planted area.

The experiment consists of 32 fields (50 x 50m) which all consist of a different layout and a variable number of planted subplots (gray plots in Figure 3). The planted subplots (5 x 5m) all contain a 1m² and 4m² planted marram grass area (Figure 4) in the same configuration. The amount of subplots (between 8 and 20 per field) and its spatial configuration differs for every field, which makes every field unique. As can be seen from the experimental design is that a spatial transition in subplot density is present; in the middle of the experiment the amount of planted plots is the highest while on the edges of the experiment (left-right) the amount of planted plots is lower.



Figure 4 Example of a marram grass plot (4m²)

In the middle of each field, an open area surrounded with straw bales was created mainly for recreational purposes during the Oerol festival in Terschelling (spring 2016). These straw bales were flushed away by the sea during the first winter (2016-2017). It should be noted that the Windwerk experiment is not specifically designed for this study or scientific research, where duplicates of fields would be desired in order to study different external variables. Although many duplicates of the small subplot fields exist, this study will only study field-scale (50 x 50m) development.

2.2 Data collection

After the Windwerk project was established (May 2016) six UAV flights were carried out in the year after in order to monitor the development of dunes and vegetation. Figure 5 shows a timeline of all mapping campaigns. The time intervals between the acquisition dates are irregular and can be relatively long (+20 weeks). Because small embryo dunes are very vulnerable for erosion by wind and



Figure 5 Timeline of the six data acquisition campaigns carried out with MUMSY sensor system

water (Maun, 2009), it is therefore expected that these dunes can possibly change in a relatively short time. In this study mainly seasonal and yearly development will be explored.

A rotary octocopter UAV system was used equipped with the Multispectral Mapping System (MUMSY), which consists of two Canon EOS 700D camera's (28mm f/2.8). One camera captures RGB imagery with a resolution of 18 megapixels. The red channel of the second camera was modified to capture near-infrared (720nm) and resulted in a false-color output. For this research only the false-color imagery was used because it could provide additional information about the marram grass vegetation development and in order to filter vegetation from the digital surface models which are created in this study.

The aerial imagery was acquired at an altitude of 80 m with a speed of 4-5 m/s, taking images every second. All images had an overlap of about 70 percent which is necessary to align all photo's. For every campaign three flights of ± 10 minutes were needed to cover the complete study area. The UAV was auto-piloted to have the same flight paths for every campaign. An overview of the flight paths is shown in Figure 6. Every mapping campaign resulted in 900-1200 images. Six ground control points were permanently places on elevated poles within the Windwerk area (Figure 7). These referencing panels, together with three permanent beach poles were accurately measured with an RTK in order to georeference the imagery with coordinates. Before every take-off, a Spectralon reflectance panel was measured by the MUMSY cameras for later radiometric corrections. During the last flight campaign (June 2017), the Spectralon panel was missing. Therefore, a white sheet of paper was used to capture its spectral reflectance for later calibration.



Figure 6 Flight paths for data collection visualized with GCP locations



Figure 7 Image of fixed elevated referencing marker within the study area

All acquisition campaigns were carried out during calm weather conditions with wind speeds below 8 m/s. The acquisition campaign of August 2016 was flown early in the morning, which resulted in extensive shadow effects behind dunes and vegetation. This often results in difficulties in photogrammetric applications and could affect the resulting digital surface model, because information in shadow areas may be lost (Yandong Wang, 2001).

2.3 Data processing workflow

Early 2017, two PhD researchers (Nolet and van Puijenbroek) from the Wageningen University published two articles about a UAV-based approach to monitor interactions between vegetation and dune/sand burial processes on two different locations within the Netherlands (Nolet et al., 2017; Van Puijenbroek et al., 2017). In their studies, the same MUMSY sensor was used which has been used for the Windwerk monitoring. Because of the similar environmental conditions and used sensor, the main data processing approach of Nolet and van Puijenbroek was applied in this study. This includes the complete pre-processing workflow from Nolet and van Puijenbroek. Also the structure from motion workflow as well as the vegetation filtering steps are mostly identical by the method of Nolet and van Puijenbroek. However, additional steps and optimizations were needed for this study to get the desired result.

Figure 8 shows a conceptual model of the most important steps applied in this study. This model can be roughly divided into; 1) methodology for data processing of UAV imagery (objective 1); and 2) analysing dune development processes over time (objective 2).

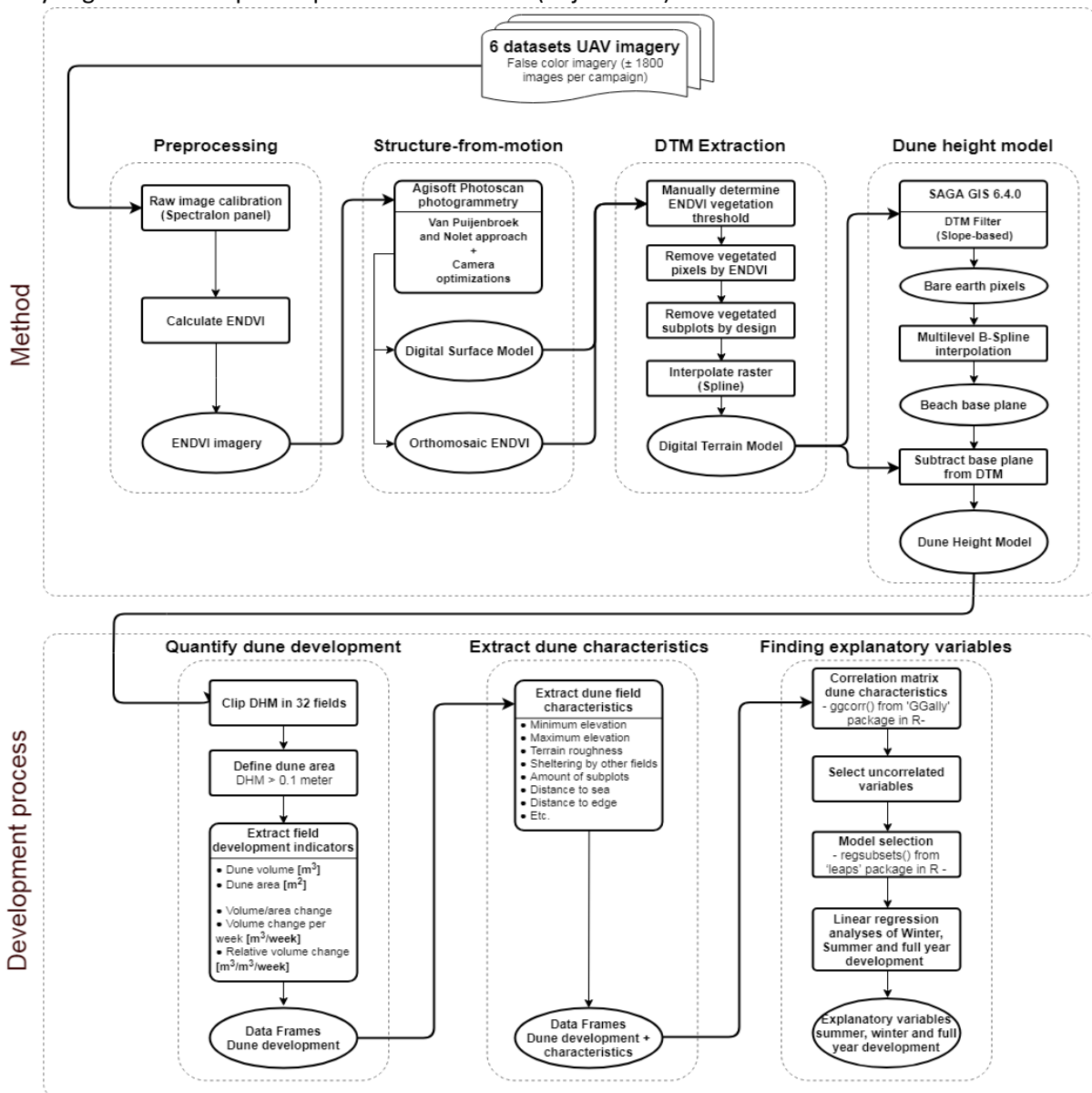


Figure 8 Conceptual model of data processing workflow and research steps

2.3.1 Pre-processing

Radiometric calibration

In order to process all images equally over time, radiometric calibration is needed to calibrate the UAV output imagery. A MATLAB script was used in order to automatically calibrate all images, which was already developed for the calibration of the MUMSY data. The calibration was done in two steps as described by (Suomalainen et al., 2014). First, all individual pixels of the sensor were calibrated by converting the digital numbers (DN) to radiance (L). This was done by a flat field and pixel-wise dark current calibration. Secondly, changes in incident irradiance of different acquisition flights were corrected. Each individual image was calibrated based on the measured reflectance of the Spectralon panel with a known reflectance curvature. This resulted in reflectance factor images (.tiff) with values between 0 and 1. More details about the used calibration procedure and equations can be found the paper of (Suomalainen et al., 2014).

During the acquisition flight of June 1st 2017 the Spectralon panel was not present. Instead of a Spectralon panel with a known reflectance factor, a calibration image was taken of a white paper sheet. The spectral reflectance curve was later measured with an ASD Fieldspec spectroradiometer. The reflectance factor values were processed and integrated in the MATLAB script where after all images from that campaign were calibrated.

Vegetation indices

In order to remove vegetation from the digital elevation model later on, all calibrated images were converted into NDVI images. Because false color imagery was used, the standard NDVI equation was not possible since the red channel was replaced by near infrared. As recommended by the manufacturer of the sensor and as has been done in previous studies by van Puijenbroek and Nolet, the Enhanced Normalized Difference Vegetation Index (ENDVI) was used. The ENDVI is a modified NDVI and replaces the red channel by integrating the green and blue channel, see equation below.

$$ENDVI = \frac{((NIR + Green) - (2 * Blue))}{((NIR + Green) + (2 * Blue))}$$

Equation 1 Enhanced Normalized Difference Vegetation Index (ENDVI)

The ENDVI calculation was executed within the software environment R (version R-3.3.2). This resulted in a single band ENDVI image with values between 0 and 1. This layer was then combined with the original green and blue bands to create a 3-band color image (ENDVI, green and blue).

2.3.2 DSM generation

After the pre-processing of the UAV imagery, the images were processed in Agisoft Photoscan Pro (version 1.3.1). The Agisoft software was used to mosaic all images together and reconstruct a three-dimensional digital elevation model by using a Structure-from-Motion algorithm. All steps and software settings in Agisoft were following the workflow which has been applied by Nolet and van Puijenbroek. However, additional optimizations were needed in order to deal with some georeferencing issues and lens correction/deformation effects. The SfM workflow is briefly described below, all specific used software settings and parameters can be found in Appendix B.

The first step in Agisoft was to align all images for every individual flight campaign. This resulted in an image which consist of tie points (points that tie one image to another). These correlated points were georeferenced by a total of 9 ground control points, which resulted in a referenced orthophoto's with a total error of approximately 0.01 – 0.03 meter. These errors represent the average X, Y and Z error (distance [m]) of all ground control points (Agisoft LLC, 2016). For three datasets (June 2016, November 2016 and May 2017) the total georeferencing error was relatively high (between 0.3 and 0.5 meter). This was mainly influenced by two referencing markers (GCP's) which showed a high error. These errors were also visible in the resulting elevation models since the elevation was highly differentiated around these referencing poles. To improve the results, the referencing was redone and markers which still contained a high error (>0.5m) were removed. After improvements dataset of November 2016 and May 2017 resulted in an average error of 0.03-0.04 meter. The dataset of June 2016 still showed a significant high average GCP error (0.24m) which couldn't be improved further. Table 1 Final average GCP error [m] for every dataset showing a relative high error for June 2016 shows the final average GCP errors of the surface models which were used in this study.

Table 1 Final average GCP error [m] for every dataset showing a relative high error for June 2016. The colour intensity corresponds to the magnitude of the average GCP errors

Date	18 May 2016	16 June 2016	16 August 2016	28 November 2016	10 May 2017	1 June 2017
Error [m]	0,017067	0,247038	0,013568	0,042636	0,030566	0,027075

Camera optimization

Following the exact same SfM workflow as Nolet and van Puijenbroek resulted in unreliable results of which some digital surface models showed a doming effect. This effect was observed especially around the edges of the study area, where the surface was exponentially descending. This doming effect can especially occur when exclusively vertical imagery is used (Smith, Carrivick, & Quincey, 2015), which was the case for this study. This is caused by camera lens distortion and incorrect specification of the camera parameters within the software (Entwistle & Heritage, 2017). By trail-and-error this problem was resolved by using the camera optimization tool of Agisoft. The camera optimization tool in Agisoft calibrates the camera and corrects for lens distortion. All cameras and lenses have some amount of lens distortion which will influence the photogrammetry height estimation (USGS, 2017). This error needed to be minimized which was done in Agisoft Photoscan. Basic camera characteristics such as pixel resolution and focal length were manually filled in. All other camera optimization variables (mainly radial and tangential distortions coefficients) were estimated by the software for the first dataset (May 2016), since this dataset didn't show a doming effect. Since the same camera setup was used for all data acquisition campaigns, these camera settings were saved and imported during the processing of all other datasets. After these camera optimization was done, the camera alignment was optimized by using the 'Optimize Camera Alignment' tool.

Depth reconstruction

Subsequently a dense cloud was generated at medium quality settings. Medium quality was more than sufficient for this research and resulted in an average point density of about 500 points/m². Because of poor textures, shadows and noisy images the stage of depth reconstruction, there can be outliers in the point cloud (Agisoft LLC, 2016). Therefore, a depth filtering algorithm is integrated in the dense cloud generation stage of Agisoft. As recommended for aerial data processing, the aggressive depth filtering option was selected for this study. It could be possible that vegetation (marram grass) will be filtered from the point cloud by this depth filtering algorithm.

Output

After the point cloud was generated, a three-dimensional mesh model, digital surface model and orthomosaic was created. All processing steps in Agisoft were done in medium (quality) setting because a higher setting was too time consuming for the large datasets. More details of the steps followed in Agisoft Photoscan and specific settings can be found in Appendix B. For each dataset a digital surface model (DSM) and orthomosaic was exported with a resolution of 0.05 meter.

2.3.3 DTM generation and removing artefacts

The DSM created by Agisoft includes vegetation and does not represent the dune height for vegetated (embryo)dunes. The elevation of vegetation was removed by creating a masking layer based on the ENDVI values of the orthophoto's. Automatic methods for removing vegetation from ENDVI imagery, like k-means clustering, were not successful since for some datasets also high ENDVI values were found in non-vegetated sand patches. This was because either the vegetation density was too low to measure a strong near-infrared reflectance, and/or the near-infrared reflectance of the bare sand was relatively high. The RGB imagery of May 2017 and June 2017 showed large brown areas in between the dune fields, which might be deposition of organic matter (e.g. algae's or sediment) on the beach. These areas supposedly share similar spectral characteristics with marram grass in the near-infrared, green and/or blue wavelengths. Because of this effect, not all vegetation was removed based on its ENDVI values. Therefore, for each separate dataset a manual threshold was defined to distinguish vegetation from sand. This threshold was visually determined by evaluating the maximum ENDVI value of sand plus a small margin of about ten percent to remove all pixels with a higher ENDVI value than sand.

The vegetation mask which was created by thresholding the ENDVI values did not mask the straw bales and also didn't always contain all vegetation since in some cases the ENDVI values of sand and vegetation were not clearly distinguishable. Therefore, another masking layer was added by visually drawing polygons around vegetated plots and the straw bales. Also some artefacts which were visible in the DSM of November 2016 (explained in more detail in section 2.3.3) were manually masked. Figure 9 shows the process of the creation of the masking layer. The original DSM was then masked by the final masking layer and the holes were interpolated using a spline interpolation tool in SAGA GIS (version 2.3.2), which resulted in the Digital Terrain Model (DTM).

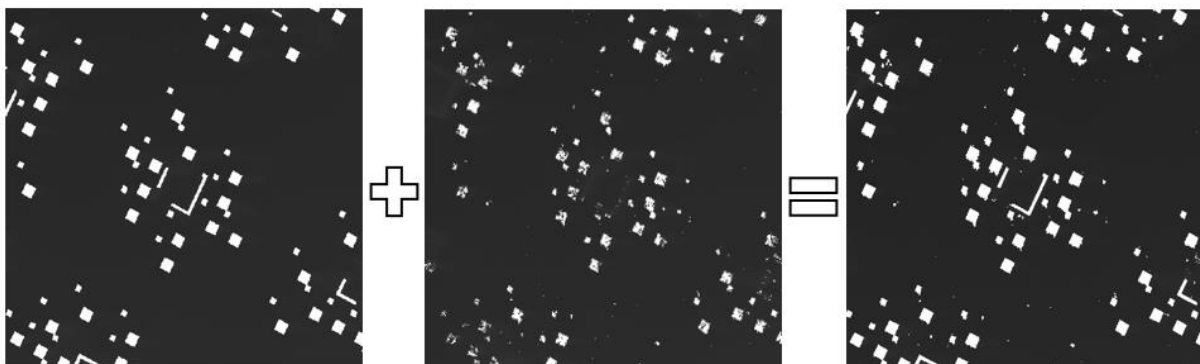


Figure 9 Generation process of DSM masking layer. Left figure showing the masking layer by original built design, middle figure shows the vegetation mask by ENDVI values and show a more speckled pattern. Right shows the final combined masking layer

2.3.4 Accuracy of DSM and DTM

In order to assess the accuracy of the DSM and DTM, field measurements were taken of the surface of embryo dunes in November 2017. This was done with an accurate RTK-DGPS device (differential GPS). It was intended to do this together with a final flight campaign to accurately compare the DTM with field measurements, but unfortunately the UAV was not able to fly due to bad weather conditions. Therefore, the RKT measurements are compared with the height of the dunes of the latest dataset (June 2017). It is expected that some variation in dune height is possible because of the temporal difference between the latest flight campaign and the field measurements.

2.3.5 Defining dunes

The DTM represents the elevation of the Windwerk soil/sand which was used to monitor embryo dune development. From this DTM the individual embryo dunes had to be defined and subtracted from the beach plane (base elevation). Embryo dunes are defined as clustered areas which have a higher elevation than the beach base plane.

First a base plane was calculated for every flight campaign. This was done by doing a slope-based filtering of the DTM which is described by (Vosselman, 2000) and is commonly used to filter digital surface models and remove objects. The idea of this filtering principle is that a large sudden elevation difference between two points is unlikely unless an embryo dune is present. Since the beach plane around the dunes in the Windwerk field is fairly flat, the slope threshold has been fixed to 2 degrees in a 1-meter radius. A cell will be classified as terrain if there are no cells within the 1-meter radius window that will exceed the maximum allowed elevation based on the slope threshold. This resulted in a scattered raster file with only elevation pixels classified as "bare earth". This raster contains a lot of NoData values which were interpolated using Multilevel B-Spline interpolation (SAGA GIS version 2.3.2) in order to create a smooth base plane that passes through the bare earth pixels. Multilevel B-Spline was used because of its large performance gains compared with normal spline interpolation. The maximum level was set to four in order to create a smooth surface with only small slopes (Appendix G).

This base elevation layer was then subtracted from the original DTM which resulted in an elevation deviation model (dune height model). From this model, calculations can be done to monitor changes in dune volume and area within the 32 experimental fields of Windwerk.

2.4 Dune development analysis

2.4.1 Dune development indicators

To explore the development of embryo dunes in relation to different characteristics (dune and terrain scale) of the embryo dunes, different indicators can be extracted from the dune fields which can explain dune development. Different indicators are used to monitor the dune development over time within all 32 individual experimental field 50x50m.

All six dune height models were clipped into the 32 individual field to monitor the development per field. These raster files were imported in R to do further calculations and analyse the development over time. From the DHM's two directly related indicators of dune development were extracted. For every dataset (flight campaign) and for each individual field, the total dune volume (m^3) and dune area (m^2) was extracted. The dune area was classified as area of which the dune height was bigger than 0.1

meter. Elevation differences smaller than 0.1 meter are most likely temporary small sand ripples which are formed by wind (M. A. Maun, 2009). The total dune volume (m^3) was calculated by summing all height differences of the dune model by its pixel size (1 pixel = $0.0025m^2$). This resulted in six data frames containing dune development information per field.

2.4.2 Dune development over time

A varying time-interval exist between the UAV datasets of Windwerk, ranging from 3 to 23 weeks. To monitor embryo dune development over time it is important to correct changes for the number of weeks between the flight campaigns. The absolute changes in dune volume ($m^3/week$) are calculated by subtracting the total dune volume per field from the dune volume from the previous campaign, divided by the number of weeks between the two campaigns.

Because the amount of initial planted subplots is varying, also the relative change irrespective of dune volume ($m^3/m^3/week$) was calculated to explore the development independent of the initial dune size. The relative volume change was calculated by dividing the absolute change by the total dune volume of a field of the previous campaign. Besides the absolute and relative volume changes, also the absolute and relative area changes were calculated in the same way.

Meteorological conditions

In order to link dune development of de Windwerk project to natural processes, it is important to have an insight of the weather conditions prior to every data acquisition campaign. Wind speed and wind direction have a positive effect on the sediment transport rate across a beach (Bauer & Davidson-Arnott, 2003). The geometry of the beach, beach width, and the wind direction will influence the fetch distance over which the wind is blowing. This fetch distance in combination with the wind speed and moisture content of the sand will mainly determine the downwind sediment transport rate (Delgado-Fernandez, 2010).

Figure 10 displays the 30-year average (1980-2010) of a meteorological weather station (KNMI) on the neighboring island Ameland. The most dominant wind direction appears to be west-southwest. Winds from this direction also display the highest wind speeds. Since the Windwerk experiment is southwest oriented, it is expected that wind from these directions (perpendicular wind) will have the biggest impact on changes of the Windwerk dunes. Daily weather data of Terschelling was briefly analysed and described.

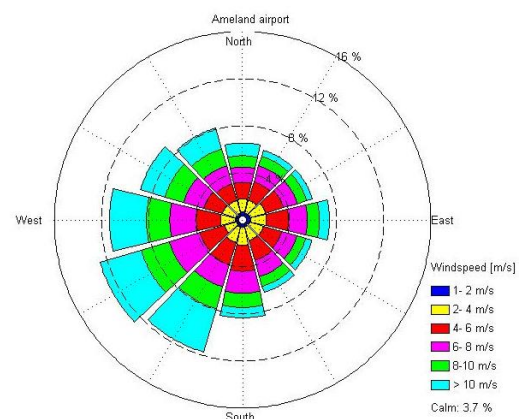


Figure 10 30-year average wind rose of weather station of Ameland (NL) - KNMI

2.4.3 Explanatory variables

To explain what factors are influencing dune development of the Windwerk project, different explanatory variables were extracted from the DTM and DHM. The explanatory variables can be divided in dune characteristics (height, size etc.) or terrain characteristics (position, elevation etc.). A manual variable selection was done based on the correlation coefficients between the variables. Sets of variables (like minimum, maximum and mean elevation) which are highly correlated (mutual

correlation higher than 0.60) were removed and only one remaining uncorrelated variable was used to study dune development. The following explanatory variables were selected for this study:

Variables which describe the terrain characteristics

Mean elevation: The mean elevation of every field was taken and added as variable. The mean elevation varies between 2 and 4 m+NAP and is correlated with the distance to the sea. Dunes at a higher elevation on the beach are possibly better protected against floods and sediment transport might be different at different elevation levels.

Roughness: Many different algorithms can be used for calculating terrain roughness from a DEM (Cooley, 2015). For this study, the surface roughness was calculated as the mean deviation of the terrains' surface. The roughness of a terrain may influence dune development. Terrain roughness has a square root relation with the sediment transport rate because it influences shear stress by wind (Reim, 2013) and areas with limited terrain roughness can develop longitudinal dunes (Gabler, Petersen, & Trapasso, 2006).

Position on the beach: The position on the beach may have an effect on the erosion and sedimentation rate of dunes. Depending on the wind direction, dunes may catch a lot of wind or sediment or are sheltered by other dune field. Because the experimental design consists of squared fields, three different directions were taken into account. In order to quantify the position on the beach in an explanatory variable, three different position codes were added to each field: 1) distance to sea, 2) distance to edges, and 3) diagonal distance (Figure 11).

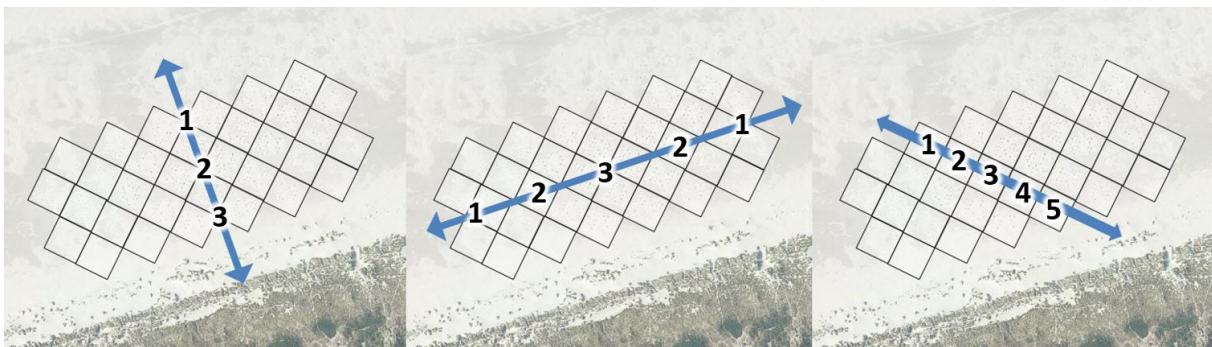


Figure 11 Position index codes with 1) distance to sea, 2) distance to edges, and 3) diagonal distance

Variables which describe the dune characteristics

Maximum dune height: The maximum dune height of every field extracted from the dune height model. Dune height might explain dune development since higher dunes are more resilient to erosion by waves and storm surge effects (Sigren et al., 2014).

Standard deviation of DHM: In addition to the terrain roughness, the standard deviation of the dune height model is taken as explanatory variable. This variable describes the variance of the height of individual dunes within a field. A high standard deviation can indicate a large amount of individual dunes, while a low standard deviation indicates a more uniform dune area.

Sheltering: Depending on the wind direction and the position of the field within Windwerk, some fields are sheltered behind other fields. This may affect the sediment rate and erosion resistance of a field. For each field the number of direct surrounding fields is calculated and added as explanatory variable.

Initial amount of planted subplots: Each field within Windwerk is unique in its spatial distribution and has a varying amount of subplots. The amount of subplots within a field is varying between 7 and 20. As can be observed from the design layout (Figure 3), fields in the centre of the Windwerk extent contain a higher amount of subplots than fields towards the edges. The amount of subplots can contribute to sheltering effects of dunes within a field. Additionally, dunes within a field with a high subplot density may also merge together when dunes are developing which make them more resilient.

2.4.4 Statistical analysis

The average overall dune development (absolute and relative) was studied over a full year (May 2016 – May 2017) and also seasonal changes between summer (May 2016 – August 2016) and winter (November 2016 – May 2017) are compared. For these three periods relations were studied between dune development and different explanatory variables by performing a multiple linear regression analyses in R (version R-3.3.2).

Changes in dune volume and dune area are both indicators for dune development. Since dune volume changes show a larger variation over time, dune volume was chosen as indicator of dune development. To study the relations irrespective of the initial amount of planted dune plots and dune size of a field, dune volume was corrected by its initial dune volume which resulted in a relative dune volume change in $m^3/m^3/week$. The relative dune change was used as depended response variable for which the independent explanatory/predictor variables are compared.

For each period (summer, winter and full year) the initial conditions at the start of that period were used for the explanatory variables. For the multiple linear regression analyses in R the statistical function “lm()” was used, which is a standard function in R for fitting a linear model. All models were performed by first using a full model and a secondly a selection of explanatory variables. The model selection was used in to exclude irrelevant variables which make it easier to interpret the model. For the model selection, the regression subset selection function (regsubsets() from ‘leaps’ package) in R was used. This function returns the adjusted R-square, Mallows's C_p , and Bayesian information criterion (BIC) for a 1 to 6 predictor model. Were a high adjusted adjusted R-square and a low BIC and C_p is preferred. Based on these values a best subset of predictors was chosen and then analysed in the multiple regression analysis.

Based on the statistical analysis, possible explanations and relationships were analysed for embryo dune development in the Windwerk experiment. For the most important variables, scatterplots were used to study if a one-to-one linear relation exists between dune development and the explanatory variable.

3 Results

In this chapter the results of this study are presented and described. Section 3.1 shows the results and products from the applied method to create a digital dune model from UAV imagery. In section 3.2 the embryo dune development of the Windwerk experiment is described which will give an insight in the dune development over time and underlying drivers which have an impact on the development.

3.1 Quantifying embryo dunes from UAV imagery

The data processing workflow as described by Van Puijenbroek and Nolet was applied in this study, but needed additional steps in to create a reliable terrain model. First, optimization was needed in the workflow of van Puijenbroek to create a digital surface model in Agisoft Photoscan. Calibrating the imagery for lens distortion by using the camera optimization tool in Agisoft was necessary after the surface models showed a doming effect associated with large GCP errors.

Also, the ENDVI imagery which was created in the pre-processing did not clearly distinguish marram grass from soil/sand. Therefore, removing vegetated elevation pixels based on ENDVI values was not accurate enough to remove all vegetation. A more detailed description of this effect is described in paragraph 3.1.2.

3.1.1 DSM from structure from motion

Although all datasets were processed equally, still inconsistencies exist in the created surface models. Looking at the average GCP errors of Table 1, the models of May 2016 and November 2016 show relative large errors. This is also visible in the cross-sections of Appendix D, where elevation anomalies can be observed compared with the previous and following cross-sections. Further optimization of the DSM's and minimizing the errors in Agisoft was not possible.

All six DSM's created in Agisoft Photoscan were exported with a pixel resolution of 0.05m (Appendix C). Looking at the DSM's, all 32 fields are clearly visible as higher elevated areas containing small dunes (Figure 12).

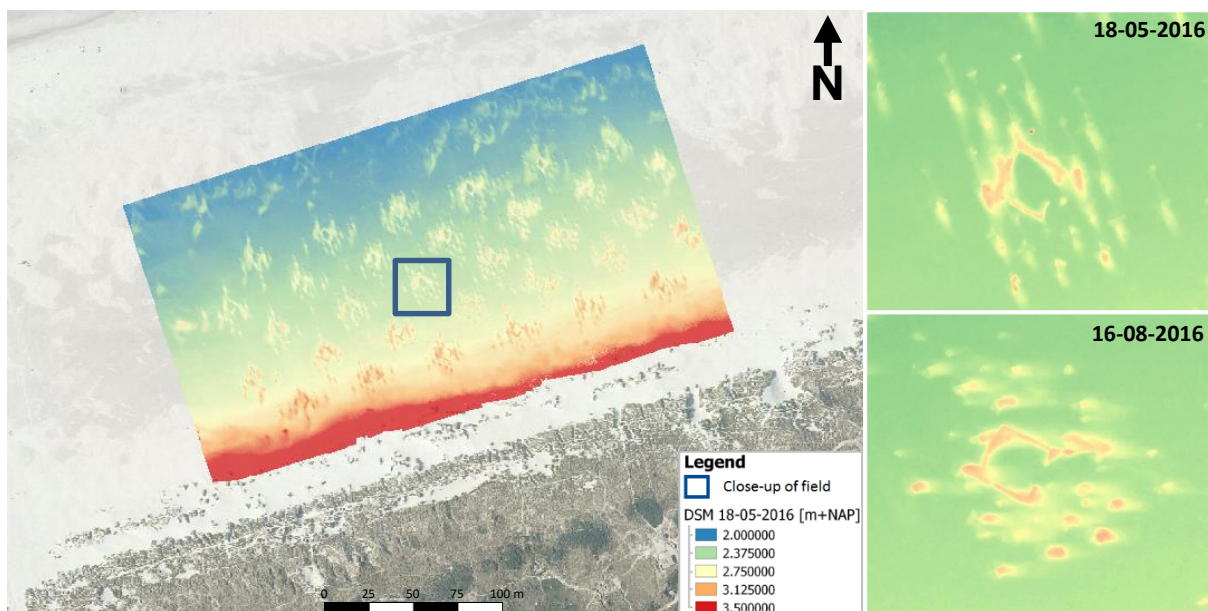


Figure 12 Digital surface model created by structure-from-motion. Left) DSM of May 18 2016. Right) close-up comparison of selected field at different moments, showing temporal differences and sand shadow effect of dunes.

The dune field on the right of Figure 12 show temporal differences of sand deposition behind vegetated areas/embryo dunes. In between the dunes the surface is smooth and flat but on the lee side of objects (vegetated plots, dunes and straw bales) sand will accrete due to sheltering. Depending on the height and density of the object or vegetation and the main wind direction, deposition will take place on the lee side. This sand 'shadow' effect is visible in all digital surface models and the direction of this is very variable. All raw digital surface models are presented in Appendix C.

Since the downwind sand shadow effect is very variable in space and time, this cannot be not directly related to long-term dune development. However, over time the centre elevation of the dunes will increase and the overall dune patches are getting larger. Figure 13 shows two cross-sections of a dune field of May 2016 and November 2016. Biggest differences in elevation can be found in the areas in between the individual dunes, which indicates that the dune field is growing. Sand will accumulate in the areas in between the dunes which will cluster different dunes and one large dune system will grow.

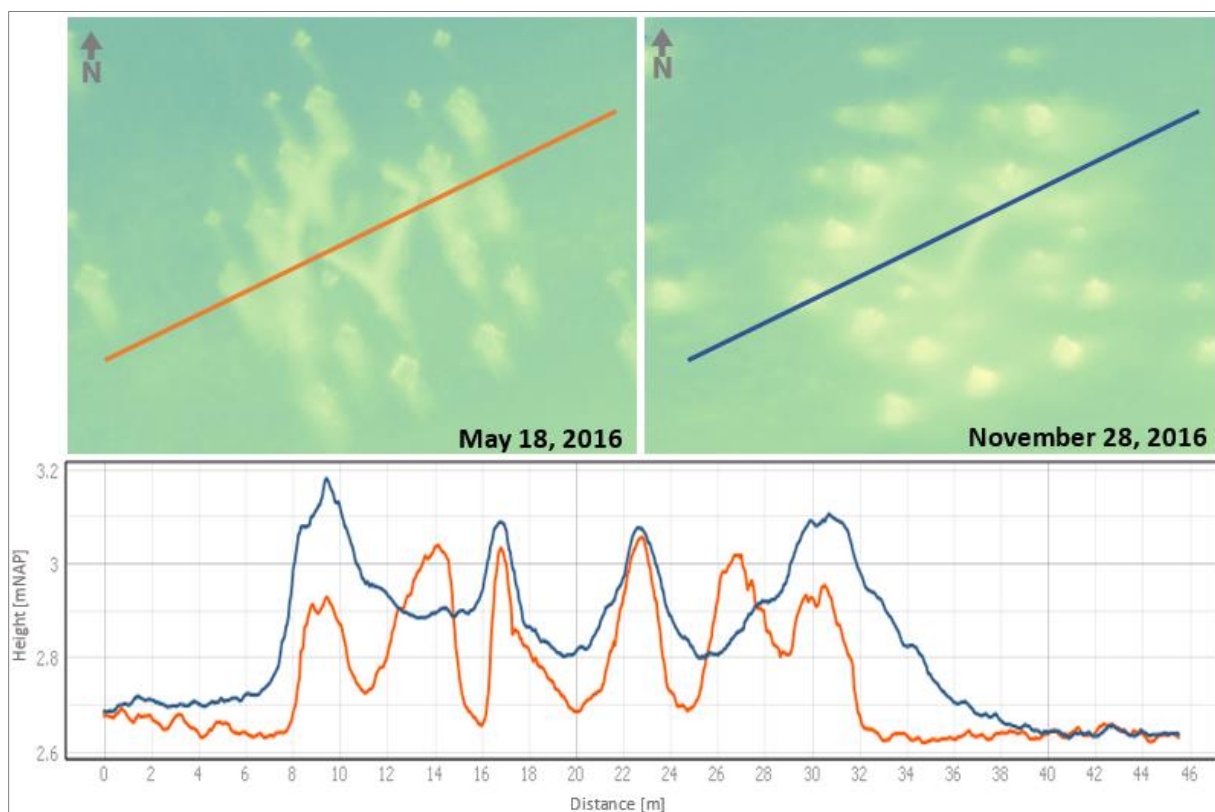


Figure 13 Cross sections of dune field (field number 23 – Appendix F) of May 2016 (orange) and November 2016 (blue) showing elevation differences especially in between the individual dunes.

Artefacts

The cross-sections of Appendix D showed anomalies in the elevation of the beach planes of June 2016 and November 2016. Besides this error, some artefacts can be found when looking at the DSM of November 11, 2016. Figure 14 shows some pit holes at the north-side of dunes. This is the result of extensive shadows behind the dunes because the data on this date was obtained in the early morning while the sun was still low. Because of the dark shadows behind the dunes, Agisoft had difficulties with matching pixels.

The resulting point cloud in Agisoft showed only a few scattered low-lying points in these areas. When creating a DSM in Agisoft, these areas are interpolated and result in these artefacts. Adjusting the quality settings in Agisoft did not improve the result, suggesting the source of the error cannot be solved within the software of Agisoft Photoscan. The visible artefacts were manually masked by drawing polygons around these areas, and later interpolated to create a digital terrain model.

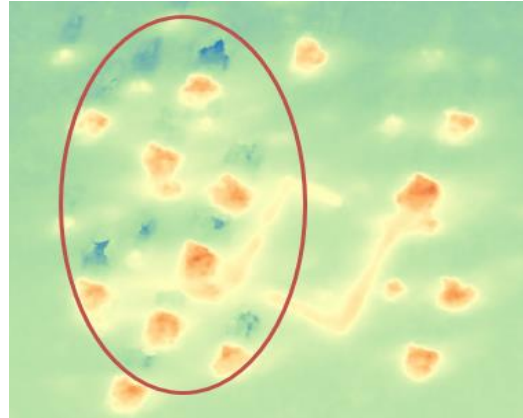
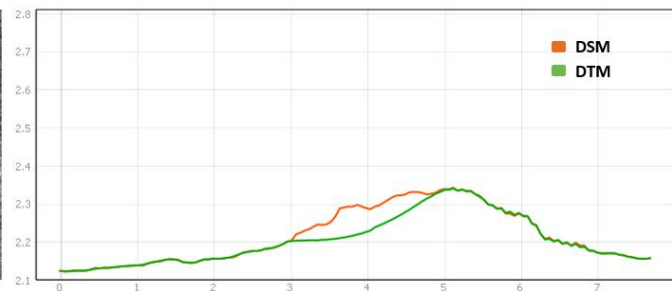
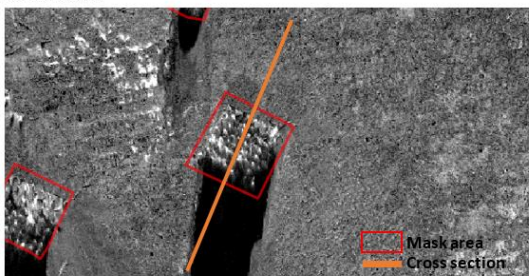


Figure 14 DSM from November 11 (2016) showing artefacts behind caused by shadow areas behind dunes

3.1.2 DTM creation from DSM

The vegetated areas of the DSM's were masked and interpolated to create the final DTM's. Spline interpolation was used in order to create a smooth natural surface representing the terrain underneath the vegetation. The contribution of vegetated areas (with unknown terrain elevation) to the total dune area of each dataset ranged between 29.95 percent (May 2016) to 11.51 percent (May 2017). Figure 15 shows a cross-section of a dune from two datasets (June 2016 and November 2016), showing differences between the DSM and DTM. Looking at both cross-sections, a much larger difference between the DSM and DTM is visible for the dataset of November 2016. The difference between the DSM and DTM of June 2016 is relatively small ($\pm 0.10\text{m}$), which is probably due to the low vegetation density in the early stage of Windwerk. Since Agisoft Photoscan already uses a depth filter when creating a point cloud, the effect of vegetation with a low density on the resulting DSM is already relatively small.

06-06-2016



28-11-2016

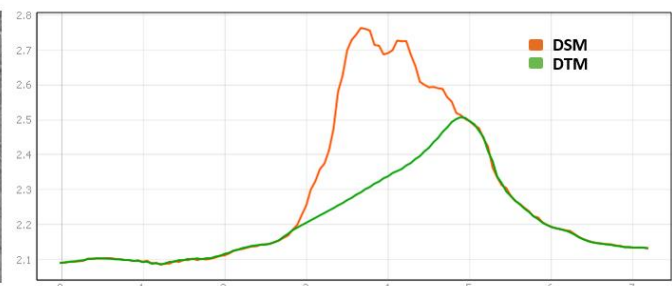
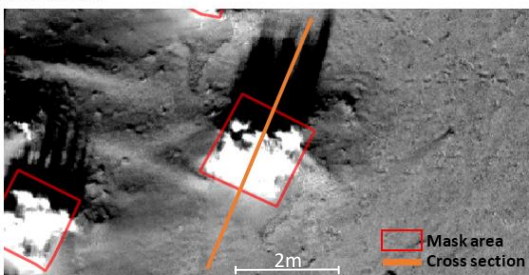


Figure 15 Left) ENDVI image of dune compared in time; Right) Cross-sections of the same dune on different moments showing differences between DSM and DTM

The left images of Figure 15 show the ENDVI imagery of June 2016 and November 2016. From these images can be concluded that the vegetation has developed between June and November, and that this had a significant effect on the resulting DSM.

Reference measurements

Creating the DTM by interpolating removed elevation points from the DSM, could lead to structural over- or underestimating of the exact terrain underneath the vegetation since information within vegetated dunes is lost. End of October 2017 a total of 300 height measurements were taken of the dunes within Windwerk. Since there is no available UAV dataset of that same moment, these measurements were compared with the latest available dataset (June 2017). Comparing the measured elevation of October 2017 with the created DTM from June 2017 resulted in an average elevation difference +0.24 meter with a standard deviation of 0.30 meter.

Figure 16 shows all sample points which are coloured by the elevation difference between the RTK measurements of October 2017 and the latest DTM (June 2017). Positive and negative elevation differences are mostly spatially clustered which might indicate that some dunes eroded and other dunes accreted. Because of the time gap of four months between the two datasets, some changes in elevation are plausible and therefore no further conclusions can be drawn on the accuracy of the derived DTM's.

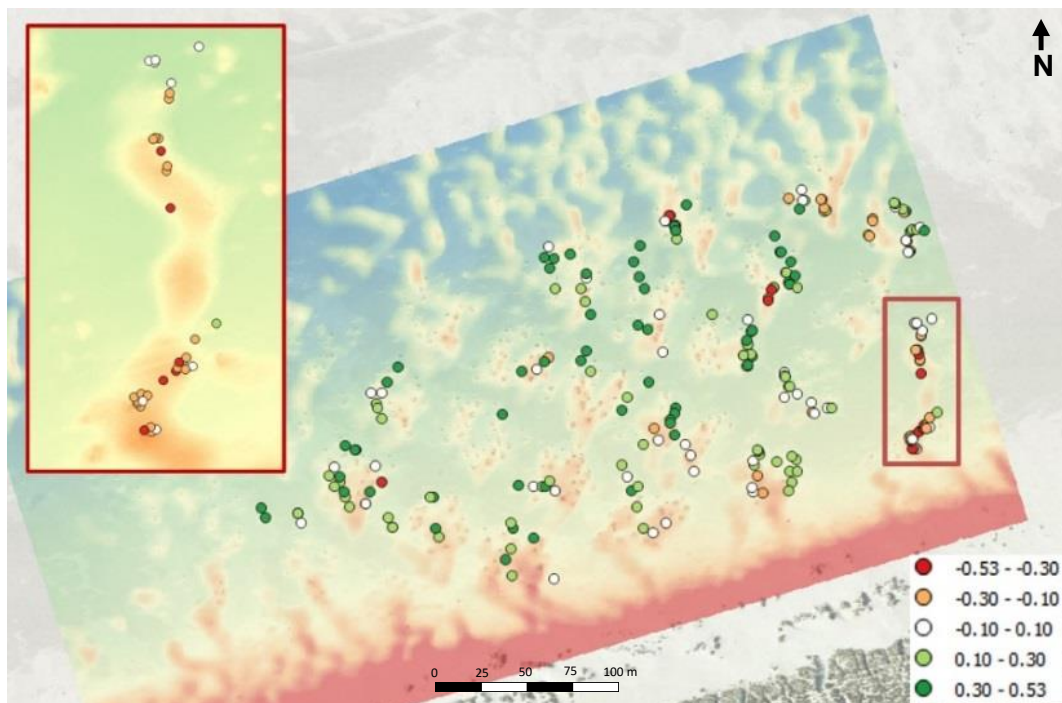


Figure 16 Elevation differences between DTM of June 2017 and RTK height measurements acquired on October, 27th 2017.

3.1.3 Creating dune height model

Because of some georeferencing issues as described in 3.1.1 and visible anomalies of the cross-sections of Appendix D, the reconstructed digital terrain models could be slightly warped and not accurately represent the true absolute elevation. When extracting the dune height model by removing the beach base plane from the DTM, these anomalies are removed and only the elevation of the dunes are derived. Figure 17 shows the differences between the DTM (left) and the DHM (middle) over the full width of the study area.

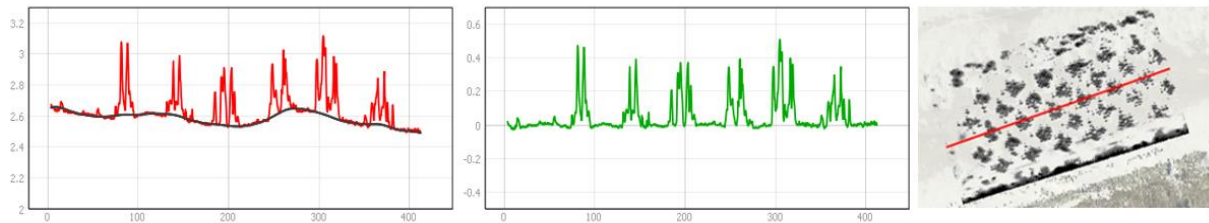


Figure 17 Cross-section showing differences between DTM and DHM. Left figure showing a cross section of the deformed digital terrain model [m+NAP] of May 2016. The middle figure shows a cross section of the derived dune height model representing the absolute dune height [m].

From the digital terrain model a beach base plane was calculated which resulted in a smooth surface model. This model was then subtracted from the DTM which resulted in the final dune height model (DHM). Figure 18 shows the resulting DHM (black) of May 2016 on top of the base plane (see Appendix E for all DHM's). From the DHM's, all 32 fields and individual dunes within Windwerk are clearly visible. From these models the dune development is measured, analysed over time and related to different aspects and characteristics.

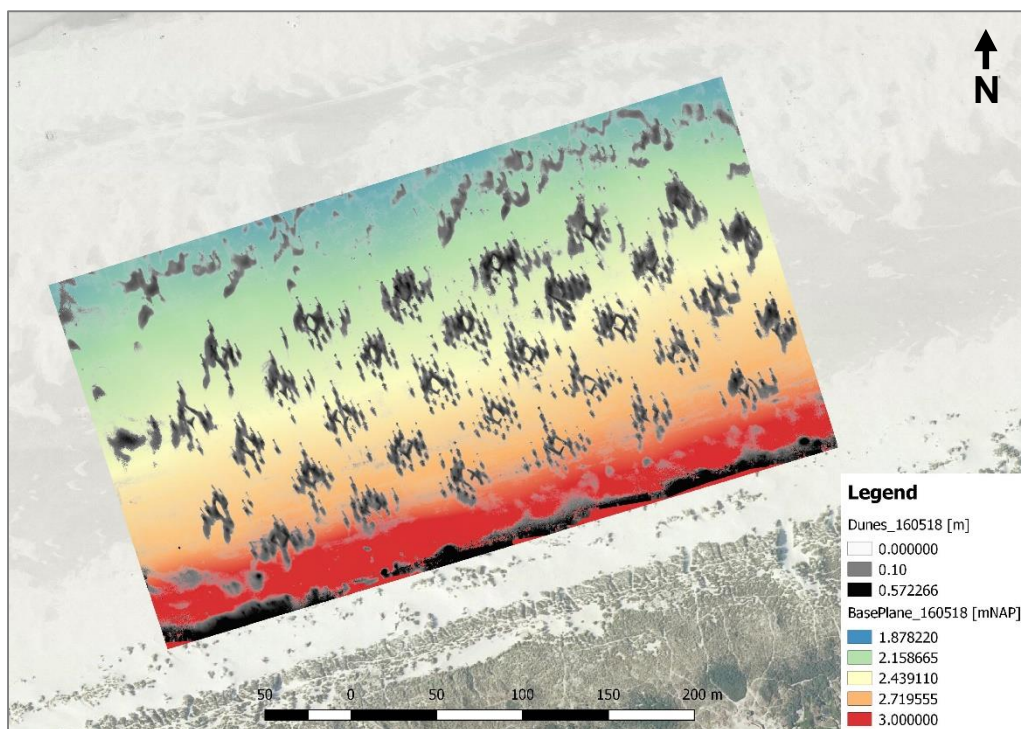


Figure 18 Dune model of May 2016 visualized (in black) on top of the beach base plane

3.2 Dune development

3.2.1 Weather conditions

Because morphological processes are driven by the effects of wind and water, it is important to know what the weather conditions were between the UAV acquisition campaigns. Appendix A shows an overview of the daily maximum wind speed, sea water level, and wave height prior to all data acquisition campaigns (April 2016 – July 2017). This paragraph gives a brief description of the weather conditions in between the different data acquisition campaigns.

May 2016 – June 2016

Around the first two data acquisition campaigns (May-June 2016) weather conditions were quite calm with no remarkable high wind speeds or water levels.

June 2016 – August 2016 – November 2016

Between June, August and November 2016 some events with wind speeds around 12m/s were recorded. It is expected that the wide beach of Terschelling shows a sedimentation effect during storms instead of erosion (Wang, 2014). The sea water level was still 0.5m below the minimum elevation of the Windwerk field and thus was not flooded or eroded by the sea.

November 2016 – May 2017

Between November 2016 and May 2017 a large time gap exists in which a lot of high wind speeds (> 16 m/s) and high water levels were recorded. In January 2017 a storm took place which coincides with extreme water levels of above +2 mNAP. This means that in combination with the high wave height the Windwerk field was completely flooded. The effect of floods on embryo dunes is not known but it is expected that most dunes will erode during this extreme event. After this storm event, quite some days were recorded with relatively high wind speeds which would imply a high sediment transport rate and thus a high embryo dune development.

May 2017 – June 2017

The conditions between the last two campaigns were stable with no remarkable values. It is expected that only small changes in embryo dune development can be found.

3.2.2 Changes in (embryo)dunes over time

Visible development

Short-term differences between different DHM's are mainly expressed by the different directions of the dune shadows, as can be seen in Figure 19. Dependent on the recent prevailing wind direction these shadows rapidly develop and change over time (<1 month).

Small differences can be found in the first four datasets (May 2016 – November 2016), which are mainly visible in the direction and length of the sand shadows. Between November 2016 and May 2017 big changes can be observed between the DHM's (Appendix E). Because of the storms, the prolonged time interval, and high sea level of January 2017, big changes were expected. In January 2017 Windwerk was completely flooded which could have a big effect on the erosion and sedimentation of embryo dunes

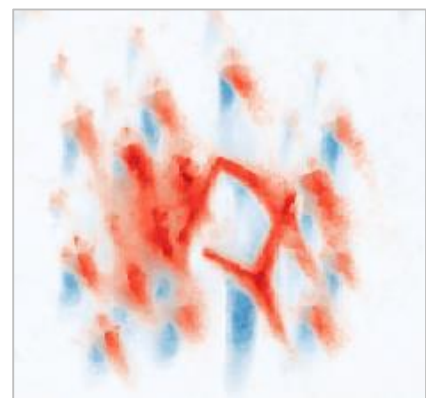


Figure 19 Dune changes between May 2016 (red) and August 2016 (blue)

within Windwerk. The DHM's of May and June 2017 both show a similar transverse dune pattern in- and outside the Windwerk field. Transverse dunes are linear dunes which generally grow under strong wind conditions with a predominant wind direction (D. W. T. Jackson, Cooper, & Green, 2014). This effect seems to partially overrule the internal processes within the Windwerk field. However, still the individual fields are visible and the transverse dunes tend to develop around the originally created dune fields.

Looking at the DTM cross-sections of Appendix D, development in the dune height and dune size can be found. The cross-sections show that dune patches are getting less spiky over time, which is the result of clustering of small dunes, as shown in Figure 13. Also notable are differences between the cross-sections of 2016 and 2017. When the Windwerk area was completely flooded during the winter, it is expected the dunes eroded. Still, all dune fields are visible in the cross-sections of 2017. When looking at the edges of the study area/cross-sections, a decrease of the elevation can be found for the DTM's of 2017, while the base elevation within the study area is stable. This means that erosion happened around the edges of the experimental area (and possibly along the whole beach), while the beach plane within Windwerk is stable.

Overall absolute development

All DHM's were clipped in 50 by 50 meter fields to study the dune development of the individual fields with different characteristics (see Appendix F for the field layout). Figure 20 show the overall development (size and volume) of all fields over time. From the boxplots can be observed that the overall mean dune area and dune volume increase over time. Also the variation in minimum and maximum values and the interquartile range is decreasing over time.

However, the DHM of June 2016 is diverging from the other datasets in both dune area and dune volume. While a relative short time-interval exists between the dataset of May 2016 and June 2016, still a significant decrease can be observed. Looking at the meteorological conditions during that time, no explanation for the erosion can be found. It is notable that the variation of dune volume of all fields on June 2016 is very low while the dune area shows a bigger variation.

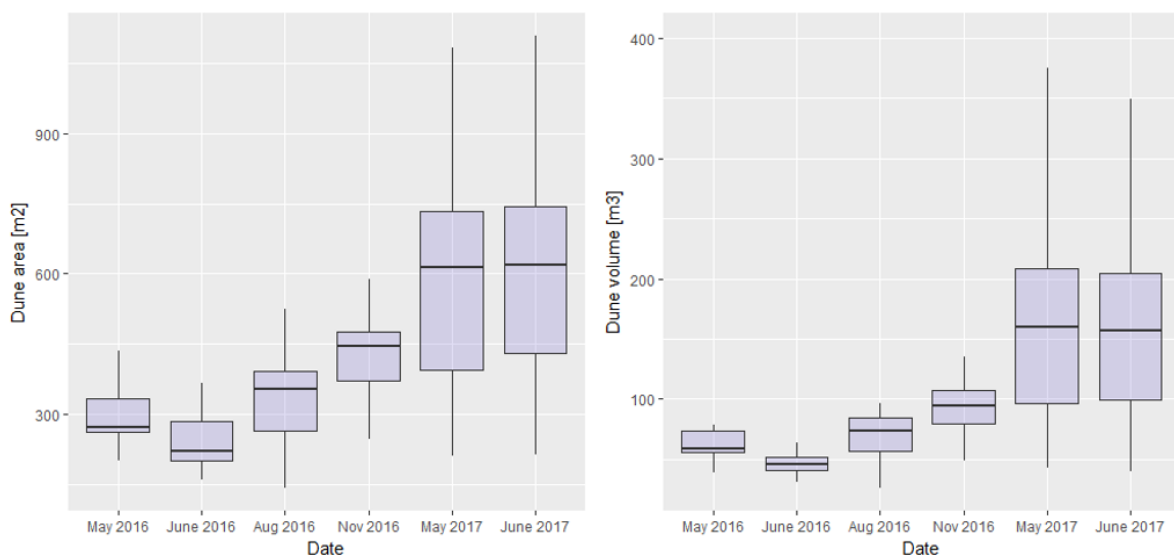


Figure 20 Boxplots of dune area (left) and dune volume (right) over time. The horizontal middle line represents the first quartile (mean). The coloured boxed represent the interquartile range (IQR) which is the range between the 25th and 75th percentiles. The whiskers show the minimum and maximum values.

Relative volume changes

To get an insight on the relative embryo dune development of each individual field irrespective of the time interval between datasets and initial dune volume, the changes in dune volume were corrected. The boxplot of Figure 21 shows the relative dune volume change ($m^3/m^3/week$) of individual fields over time. From this figure can be concluded that volume changes between May - June 2016 are all decreasing except two outliers. June - August 2016 show the biggest increase in relative dune volume and has also the largest range of variation, some fields are strongly growing while others are eroding.

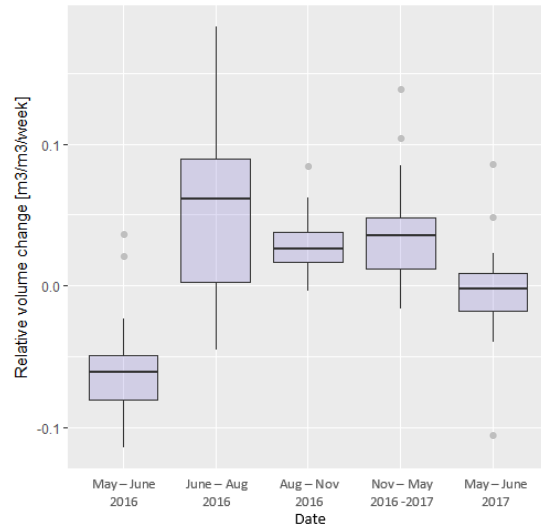


Figure 21 Boxplot of relative dune volume changes ($m^3/m^3/week$). The coloured boxed represent the interquartile range (IQR) which is the range between the 25th and 75th percentiles. The whiskers show the minimum and maximum values of max $1.5 \times IQR$. The points represent the outliers.

The relative volume changes between May – June of 2016 and 2017 are both (mostly) negative and lower than the other observations. However, in May – June 2017 some fields are still increasing in volume. The weather conditions between the datasets were both fairly calm with no special events.

Spatial variation of dune development

Figure 22 show bar graphs of the total dune volume (left) and the relative dune volume changes (right) over time. On the left figure some clear spatial patterns can be found. The fields on the north side of Windwerk contained the largest dune volume in 2017. This is mainly caused by the transverse dunes which were mainly prevailing seawards. Furthermore, it is visible that some fields on the edges of Windwerk (west-east) didn't show any significant changes/development over time. These dunes and its vegetation were probably suffering from the direct influence of the wind. Vegetation within some of these fields also disappeared completely over time.

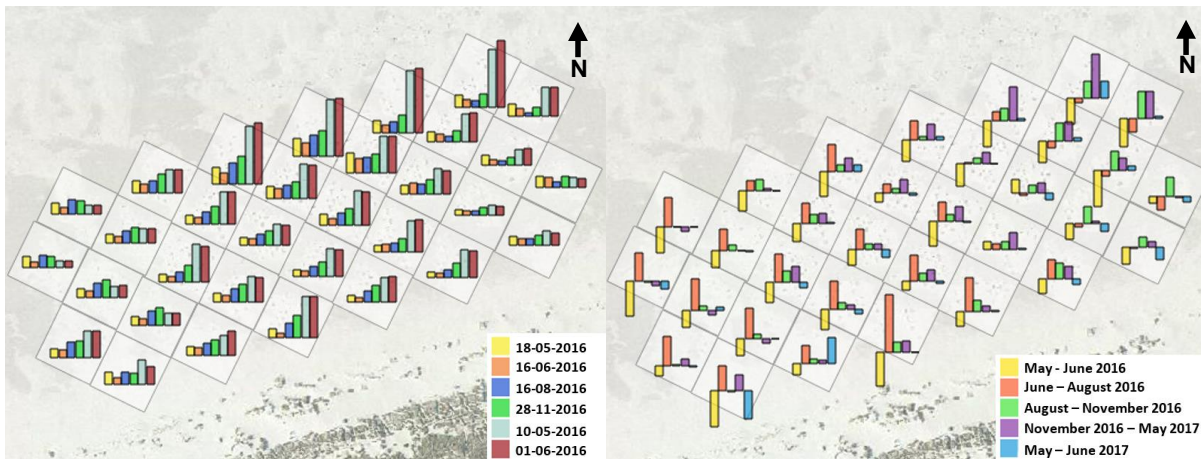


Figure 22 Left: Bar graphs of total dune volume changes [m^3] per individual field. Right: Bar graphs of relative dune volume changes [$m^3/m^3/week$]

From the right figure can be observed that the relative dune changes of June – August 2016 is positive for most fields. Dune development of fields in the west is relatively high, while fields in the east are decreasing in volume. The opposite pattern is visible when looking at the changes between August 2016 and May 2017. Fields in the north-east of Windwerk show an overall higher increase in dune volume than other fields.

3.2.3 Statistical analyses

Dune development of all fields was related to various explanatory factors in order to get an insight of key factors which are influencing dune development. To discover relations with dune volume changes irrespective of the amount of dunes and the time-interval in-between the datasets, the relative dune volume change was used as response variable and indicator of dune development.

Relations with dune development were studied for three different periods; 1) spring-autumn, 2) winter and 3) full year. Because of the significant transverse dune effect which appeared on the datasets of 2017, relations were studied first for dune development between spring and autumn (May 2016 - November 2016) to explore relations to dune development under “normal” conditions (without the transverse dune effect). Also development during winter (November 2016 – May 2017) and development during a full year (May 2016 – May 2017) were studied to see if similarities can be found.

Table 2 Multiple regression analysis for relative dune volume changes [$m^3/m^3/week$]. The predictor values were taken from every first dataset of the studied period.

Significance levels: *** ($p < 0.001$), ** ($p < 0.01$), * ($p < 0.05$), . ($p < 0.1$)

Factors	Full model	Model selection	Full model	Model selection	Full model	Model selection
	Spring-Autumn	Spring-Autumn	Winter	Winter	Full year	Full year
Dune characteristics						
<i>Dune volume</i>	0.0901 .	0.0414 *	0.26065		0.773	
<i>Dune area</i>	0.0563 .	0.0132 *	0.41732		0.587	0.010083 *
<i>Max dune height</i>	0.5384		0.09971 .	0.055605 .	0.739	
<i>STDEV dune height</i>	0.0701 .	0.0333 *	0.26910		0.714	0.120393
Field characteristics						
<i>Subplot amount</i>	0.0971 .	1.27e-05 ***	0.78309		0.239	0.000309 ***
<i>Surrounding fields (sheltering)</i>	0.0334 *	0.0140 *	0.01844 *	0.019576 *	0.045 *	0.012319 *
<i>Mean elevation</i>	0.2069	0.0594 .	0.00703 **	0.000714 ***	0.724	
<i>Terrain roughness</i>	0.6427		0.04919 *	0.000325 ***	0.516	
Spatial position on beach						
<i>Distance to sea</i>	0.7078		0.48990		0.650	
<i>Distance to edges</i>	0.3319		0.01083 *	0.005534 **	0.615	0.230124
<i>Diagonal distance</i>	0.2320	0.0546 .	0.10191	0.111830	0.664	

Table 2 shows the results of the multiple regression analysis for the three time periods. For every period a full model and a model selection was carried out. The periods’ development was compared with the explanatory factor values of the first (initial) dataset of that period.

Spring-autumn development

For the first period (spring – autumn) the *amount of subplots* was the most important explanatory factor (predictor) for relative dune volume changes. This field characteristic indicates that a higher amount of initial planted marram grass subplots will also increase the overall growth rate of the embryo dunes within a field. Also sheltering by other fields was an important predictor for the dune development of this period.

Looking at the dune characteristics, the most important predictor is *dune area*. Noted should be that the *dune area* and *amount of subplots* are partly correlated in this stage since the dune area is mainly influenced by the planted subplots. The *diagonal distance* (North-West direction) is the most important direction factor for this period. When looking at the dune height models of this period, this can be confirmed by the orientation of the dune shadows which are varying in south to east direction.

The scatterplots of Figure 23 show the relative dune volume changes against some explanatory variables. The three scatterplots all show a positive relation to the relative dune volume changes, although the linear correlations are relatively weak. For the *dune area* at the start of the period (May 2016) a negative relation was found. Fields with a smaller initial dune area, relatively develop faster than fields with larger dune areas.

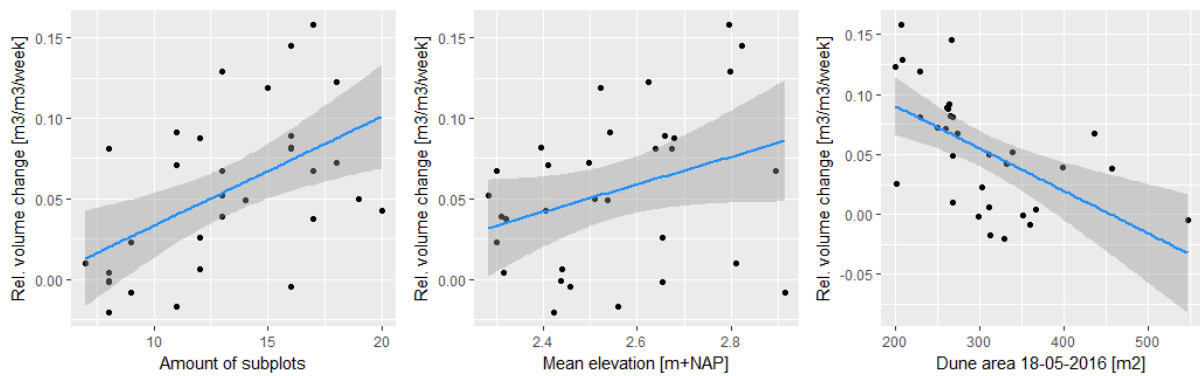


Figure 23 Scatterplots of response variable to predictor variables of the period spring-autumn 2016, showing positive one-to-one relations

Winter development

The first dataset after the winter period (May 2017) showed the predominant transverse dune effect within and outside of the experiment field. The *terrain roughness* and the *mean elevation* of a field were the most important factors during the winter period. For the *mean elevation* a negative relation was found. Fields with a higher elevation were not affected as much by the transverse dunes, and thus increased less in volume compared with fields towards the sea (Figure 24).

The terrain roughness has a positive relation to relative dune volume changes. The *maximum dune height* was the most important dune characteristic. However, no direct one-to-one relation was found when comparing the dune height to the relative dune volume change in a scatterplot.

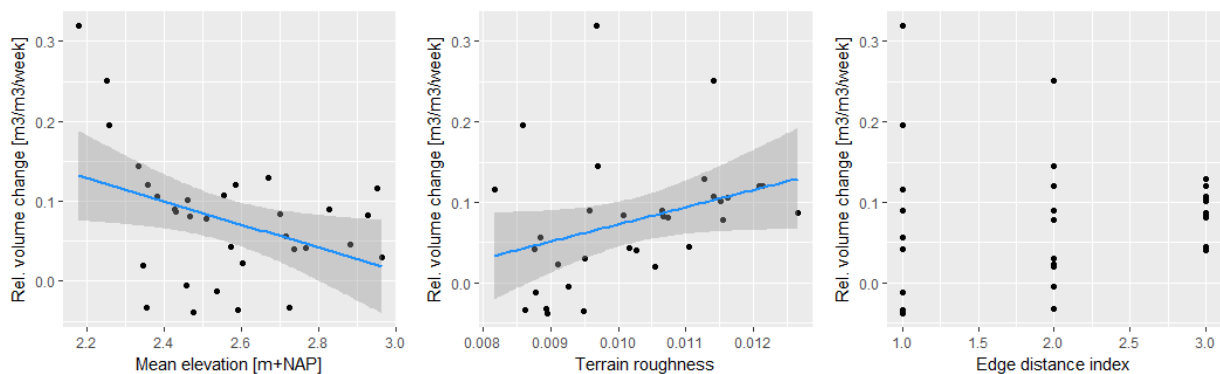


Figure 24 Scatterplot of response variable of the winter period to explanatory variables of November 2016

Distance to the edges of Windwerk was the most important direction variable. The orientation of the transverse dunes of 10-05-2017 was also in the same direction. The scatterplot of the “distance to edge” variable shows a relatively big variation in relative dune volume changes in fields towards the edges (index code 1, Figure 11), and a small variation for fields in the middle of Windwerk (index code 3, Figure 11). Fields in the middle of Windwerk were all growing at about the same rate. Fields on the edges however might develop relatively fast, but can also erode.

Full year development

The full year dune development does contain the same predominant transverse dune effect of the winter period. However, the results of the multiple regression analyses of the full year show a more similar result with the relations found for the spring-autumn period rather than the winter period. The most important explanatory factor for the full year dune development is the *amount of subplots* within a field. The left scatterplot of Figure 25 shows a positive relation between the amount of subplots and the relative dune volume changes. This means that the relative dune volume development will be higher within fields with a higher amount of planted subplots/vegetation. The most important dune characteristic is the *dune area*. This suggests that fields with large dune areas develop faster on the long term than fields with a lower dune area.

The most important spatial direction factor was the *distance to the edges* of Windwerk. This corresponds to the most dominant direction factor of the winter period and might be affected by the transverse dunes.

No linear relations were found when comparing other independent variables from the start of Windwerk (May 2016) to the development over a year (Figure 25, middle and right scatterplot)

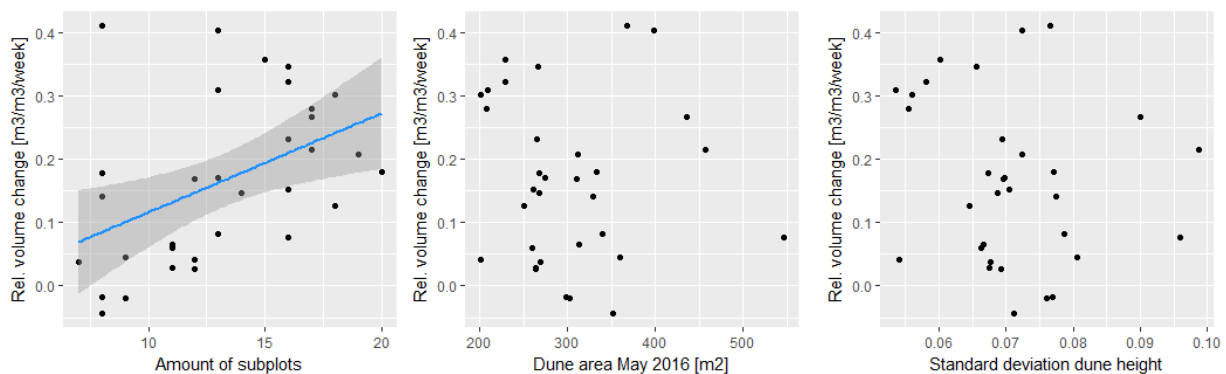


Figure 25 Scatterplot of response variable of the full-year development to explanatory variables of May 2016, showing a weak positive relation for the amount of subplots (left) and no linear relations to other variables.

4 Discussion

4.1 Creation of the DSM by SfM

Using high-resolution UAV imagery and structure-from-motion techniques, it has been demonstrated that a detailed surface model can be created to monitor dune development over time. Structure from motion techniques to create a digital surface model could rival or exceed the accuracy of laser technologies such as LIDAR (Peterson et al., 2015). However, looking at the georeferencing errors of Table 1 and the cross-sections of Appendix D, inconsistencies exist in the created DSM's. This resulted in vertical elevation deviations which were visible on the datasets of June 2016 and November 2016. Although no proof was found, a possible explanation for the large georeferencing errors as described in section 2.3.2 could be that Agisoft Photoscan had problems with referencing the elevated markers which were located on fixed poles of about +1.5 m above the surface (Figure 7). Only a low amount of tie-points was found for the elevated markers. Possibly a higher accuracy setting for aligning the imagery (creating tie-points) may improve the results. No comparable literature and/or studies was found where ground control points were located on elevated poles and therefore this cannot be compared or confirmed by other sources. All studies and literature which used and described UAV photogrammetry used ground control points and markers which were placed directly on the surface. Despite the vertical error of the DSM's, the impact of these errors on this study are expected to be small since only the dunes will be extracted from the surface. Any deformations of the beach surface will hereby be negligible.

Photogrammetry (structure-from-motion) is a proven methodology and exists for quite some time already (Rosenberg, 1955). While software like Agisoft Photoscan makes it rather simple to reconstruct a three-dimensional model from RGB imagery, complex mathematical functions are used to compute these models which can be tuned by many different settings and parameters. The used settings for this study (as described in section 2.3.2 and Appendix B) were based on similar studies of (Nolet et al., 2017) and (van Puijenbroek et al., 2017). However, the impact and sensitivity of all individual settings and parameters have not been studied in detail and also no relevant literature was found which describes the different settings (except the Agisoft user manual (Agisoft LLC, 2016)) and/or its effects. Many studies have been published which used Agisoft Photoscan to reconstruct a digital terrain model from high resolution UAV imagery, but often little is described on the specific settings which were used.

4.2 Creation of the digital terrain models

A weakness of structure-from-motion is that no digital terrain model can be created when dense vegetation is present. The digital surface models created in Agisoft Photoscan include vegetation (marram grass) which needed to be removed in order to create a digital terrain model. Figure 15 shows differences between the DSM and DTM of two different datasets. The cross section of May 2016 shows relatively little differences between the DSM and DTM. Directly after the Windwerk experiment was established (May 2016) the marram grass plots contained a low vegetation density. Later the vegetation expanded as can be seen from the ENDVI values of Figure 15. The contribution of vegetation in the two first datasets was probably too low to be captured by photogrammetry, and thus these models might already be close to a DTM. However, the exact contribution of low density marram grass to the created digital surface model is not known. It is expected that unnecessary filtering the datasets from the early stage of Windwerk will not have a big impact on the results of this study since only small changes are present.

Vegetation was masked from the DSM based on the ENDVI values of the corresponding orthomosaic. Because the manufacturer of the used sensor recommended the ENDVI vegetation indices and because this indices was also used in the study of (van Puijenbroek et al. 2017), the ENDVI was used for this study. As Equation 1 shows, the NIR, green and blue channels are used to calculate the vegetation indices. Compared to the more common NDVI, the red channel is replaced by the green and blue channel. In the comparable study of (van Puijenbroek et al., 2017), k-mean clustering was used to differentiate vegetated pixels from sand pixels. However, in this study this was not possible due to high ENDVI values from the bare earth (sand). This might be caused by organic matter (e.g. algae's or sediment) on the beach, which was visible as brown areas on the RGB imagery. Besides, the reflectance values of the green, blue and NIR spectrum from dry (yellow) sand and yellow vegetation are possibly not very distinguishable from each other. The use of a different vegetation index (such as greenness identification based indices (Yang et al., 2015)), or by integrating the red channel would possibly make marram grass better distinguishable in this case.

Because not all vegetation could be removed by the ENDVI masking layer, a second masking layer was used to mask all vegetated subplots by original design, as illustrated in Figure 9. This method was possible since this experiment contained very discrete vegetated patches (plots) and the vegetation was not expanding much within one year. However, by doing this it is possible that non-vegetated elevation pixels will be removed from the DSM and information got lost. The effect of this to the final volume balance is expected to be minimal and negligible.

The masked DSM was interpolated using Spline interpolation in order to create a smooth result which would represent the smooth surface of dunes. The accuracy of this surface estimation is not known. The used spline interpolation approach could overestimate the true surface. The reference measurements as described in section 3.1.2 show an average difference of +0.24m between the latest dataset (June 2017) and the RTK GNSS measurements of October 2017. However, of the time gap in-between these datasets no conclusions can be drawn about the accuracy of the used interpolation method. Another comparable study (Taddia et al., 2016) used GNSS measurements to help interpolate the unknown terrain underneath vegetation. For every dune an accurate measurement was taken of the highest terrain elevation of the dune. This would improve the DTM accuracy but would need many manual measurements, which is not suitable for the scale of this study.

4.3 Creation of dune height model

Figure 17 shows a cross section of the DTM and the resulting dune height model. This method was very suitable for this study because some surface models showed unlikely deformations due to georeferencing issues (section 2.3.2). The created beach base plane followed large scale deformations and warping effects whereby the georeferencing issues did not affect the subtracted dune height model. However, it could be possible that the entire beach plane of Windwerk will trap sand and raise as result of the planted vegetation. Because of the slope-based method, only the dunes above the beach base plane area studied, and not the development of the beach plane itself. Alternatively, if all elevation models are accurately referenced, base plane differences can be monitored as well to get a better overview of the total sedimentation rates.

4.4 Dune development over time

Looking at the boxplots of Figure 20, the absolute dune development of all fields is visualised in time. As expected an overall growing pattern can be found, except for June 2016. The dunes of June 2016

are smaller in size and volume compared with the first dataset of May 2016. Looking at the weather conditions between May and June 2016 (Appendix A), no extreme conditions were found which would explain the overall eroding trend. Since the dunes during the early stage of Windwerk (month after vegetation was planted) mainly consist of temporary shadow dunes as is visible from Figure 19, it is possible that a change in wind direction caused an overall eroding effect. When looking at the relative volume changes Figure 21, which are corrected for the time in-between the datasets and the initial volume of the dunes ($m^3/m^3/week$), June 2016 shows the largest variation. This might indicate that that early stage embryo dunes are very unstable and can change rapidly (both erosion and sedimentation).

Figure 20 and Figure 22 both show a big increase in dune area, volume and volume changes in May and June 2017. When looking at the DSM's of these periods large overruling dune patterns can be observed which also exists outside the experimental field. These (transverse) dunes have a large impact on the total dune volume of all fields, which is visible in the results. It should be taken into account that this dune effect might not be directly related to dune development as result of the Windwerk experiment/vegetation, because this effect was present on the entire beach around Windwerk.

Because of the large and irregular time gaps between the datasets (Figure 5) and the overall growing pattern in dune size and volume, it is hard to draw conclusions about seasonal differences in dune development. The study of (Montreuil et al., 2013) concluded that the development of embryo dunes is seasonal, with erosion during autumn and winter and dune growth in summer. This was also the case in this study, where the complete study area flooded during winter. However, as mentioned by (Wang, 2014), the beach of Terschelling is less prone to erosion than other beaches of neighbouring islands Texel, Ameland and Vlieland because of the wide beach (>200m).

Differences can be found between the key drivers influencing dune development during winter and summer (Table 2). During winter the dune height and elevation were the most important factors when explaining dune development. Whereas during summer mainly the amount of planted subplots and dune area seems to be important. The development over a full year seems to be mainly explained by summer factors. The results of the comparable study of Van Puijenbroek et al., (2017) on the neighbouring island Texel, shows a similar result, where embryo dune development was mainly explained by the amount of vegetation and sheltering. Also a group of student from the Wageningen University did field measurements of Windwerk during the summer of 2016 (Bruls et al., 2016). They discovered that the dune height and vitality of the vegetation was mainly related to the plot size ($4m^2$ are higher than $1m^2$ plots). Although the scale of their study is different (subplots versus dune fields), this means that dune size is in both cases related to the amount of vegetation.

The explanatory variables used in this study are all derived from the elevation models created in Agisoft Photoscan. Possibly other (external) variables such as meteorological data (precipitation, average wind speed, and average wind direction) or vegetation data (height, vitality, density) could be added to the regression model which might show other causal insights in dune development.

4.5 Broader implications

An important disadvantage of UAV monitoring is that calm weather is necessary in order to carry out a UAV flight campaign. Since coastal areas tend to be very windy, planning UAV flight campaigns is very hard. Because of the temporality of embryo dunes (Montreuil et al., 2013), regularly monitoring would

be preferred in this study to evaluate embryonic changes. However, as Figure 5 shows the time gaps between the data campaigns are very irregular. Especially during winter, when the most extreme weather conditions can be found and dunes change quickly, planning a UAV flight can be difficult. Although most dune fields increased in size after the winter of 2016 (Figure 20 and Figure 22), the complete study area flooded during a storm in January 2017 (Appendix A) which should have caused a lot erosion. This however was not visible in the next dataset of May 2017 due to the large time gap.

Monitoring more often and after storm events would possibly show more insights in the temporal response and erosion resistance of embryo dunes development. More prolonged monitoring would be necessary to study seasonal patterns and long-term development of embryo dunes into larger (fore)dunes.

Experimental setup

The experimental design of Windwerk consists of 32 unique fields with the highest density of subplots per field in the middle of the field, and less subplots towards the edges (Figure 3). Since the most important explanatory field characteristic of Table 2 is the amount of subplots and second the amount of sheltering by other fields, this might a combination of different variables as result of the chosen experimental design. To study the individual impact of different variables, it would be better to include duplicates of fields with a different spatial position within the Windwerk field.

5 Conclusions and recommendations

The results of this study have shown that UAV-acquired high resolution imagery can be used to accurately monitor embryo dunes over time. This provided new insights in the development of embryo dunes and main drivers influencing this development. From a method and process point of view different conclusions can be drawn.

Method

Structure from motion techniques can be very suitable for accurately reconstructing a three-dimensional surface model when full control of all software settings and parameters is used right for the specific application. This study applied roughly the same methodology with the exact same equipment as used in (van Puijenbroek et al., 2017) to study embryonic dune development along the Dutch coast. Main improvements were found in adding a lens correction step to calibrate the camera and correct for lens distortions. The resulting DSM's provide a highly detailed model of the beach's surface which can be used to accurately detect and monitor embryo dunes. However, this study showed that even when the same methodology, with equal settings and variables is applied to six equivalent datasets, a consistent vertical georeferencing accuracy cannot be guaranteed. This might be the result of the elevated georeferencing markers which were located on fixed poles ± 1.5 meter above the surface. However, by applying the beach plane correction step still good estimates of embryo dune development can be made since it adapts to any deformations of the digital models caused by the vertical georeferencing issues.

Morphological development

The development of the embryo dunes of Windwerk show an overall growing pattern over time where no significant seasonal differences can be found when looking at dune growth or erosion. Short-term dynamics are mainly expressed by the (changing) sand shadows behind dunes, whereas long-term development is expressed by accumulation of sand in between individual neighbouring dunes.

When looking at key drivers influencing the dune development of Windwerk, differences were found between summer and winter development. Summer development was mainly determined by the amount of planted grass plots and sheltering by other fields, whereas winter development was influenced by the beach elevation and terrain roughness. Most important directional factor was the distance to the edges of the experimental field (west-east) and diagonal distance, which can be explained by the predominant wind direction.

Recommendations based on this study are to further investigate the accuracy of the reconstructed digital models (DSM, DTM and DHM) by acquiring accurate RTK measurements of dune elevation within vegetation at the same day of a UAV flight. Also, to study seasonal patterns and long-term embryo dune development (of Windwerk), it is recommended to continue monitoring the dune development of Windwerk using UAV-based systems.

6 References

- Agisoft LLC. (2016). Agisoft PhotoScan User Manual. *Professional Edition, Version 1.2*, 37.
- Arnott, R. D. (2009). *Introduction to Coastal Processes & Geomorphology*. Cambridge University Press. [https://doi.org/10.2112/1551-5036\(2006\)22\[1589:BR\]2.0.CO;2](https://doi.org/10.2112/1551-5036(2006)22[1589:BR]2.0.CO;2)
- Bakker, M. A. J., Heteren, S. Van, Vonhögen, L. M., Der, A. J. F. Van, Valk, B. Van Der, Bakkert, M. A. J., ... Spek, A. J. F. Van Der. (2017). Recent Coastal Dune Development : Effects of Sand Nourishments
Stable URL : <http://www.jstor.org/stable/41508572> Linked references are available on JSTOR for this article : Recent Coastal Dune Development : Effects of, 28(3), 587–601.
- Bauer, B. O., & Davidson-Arnott, R. G. D. (2003). A general framework for modeling sediment supply to coastal dunes including wind angle, beach geometry, and fetch effects. *Geomorphology*, 49(1), 89–108. [https://doi.org/10.1016/S0169-555X\(02\)00165-4](https://doi.org/10.1016/S0169-555X(02)00165-4)
- Beniston, M., Stephenson, D. B., Christensen, O. B., Ferro, C. A. T., Frei, C., Goyette, S., ... Woth, K. (2007). Future extreme events in European climate: An exploration of regional climate model projections. *Climatic Change*. <https://doi.org/10.1007/s10584-006-9226-z>
- Bruls, A., Hermens, J., Huizing, E., Tanson, M., & Verstraeten, L. (2016). *Factors influencing dune growth and the vitality of dune building Ammophila arenaria*.
- Carter, R. W. G. (1991). Near-future sea level impacts on coastal dune landscapes. *Landscape Ecology*, 6(1–2), 29–39. <https://doi.org/10.1007/BF00157742>
- Chandler, J. H. ., & Buckley, S. (2016). Structure from motion (SfM) photogrammetry vs terrestrial laser scanning. In *The Geoscience Handbook: AGI Data Sheets, Fifth Edition*. American Geosciences Institute.
- Cohn, N. (2018). New Insights on Coastal Fore-dune Growth : The Relative Contributions of Marine and Aeolian Processes, 4965–4973. <https://doi.org/10.1029/2018GL077836>
- Cooley, S. (2015). GIS 4 Geomorphology: Terrain Roughness – 13 Ways. Retrieved October 4, 2017, from <http://gis4geomorphology.com/roughness-topographic-position/>
- de Vriend, H., van Koningsveld, M., & Aarninkhof, S. (2014). ‘Building with nature’: the new Dutch approach to coastal and river works. *Proceedings of the Institution of Civil Engineers - Civil Engineering*, 167(1), 18–24. <https://doi.org/10.1680/cien.13.00003>
- De Vries, S., Southgate, H. N., Kanning, W., & Ranasinghe, R. (2012). Dune behavior and aeolian transport on decadal timescales. *Coastal Engineering*, 67, 41–53. <https://doi.org/10.1016/j.coastaleng.2012.04.002>
- de Winter, R. C., & Ruessink, B. G. (2017). Sensitivity analysis of climate change impacts on dune erosion: case study for the Dutch Holland coast. *Climatic Change*, 141(4), 685–701. <https://doi.org/10.1007/s10584-017-1922-3>
- Delgado-Fernandez, I. (2010). A review of the application of the fetch effect to modelling sand supply to coastal foredunes. *Aeolian Research*, 2(2–3), 61–70. <https://doi.org/10.1016/j.aeolia.2010.04.001>
- Doedens, B., Spaan, M., Annema, H., Doedens, B., Floris, E., Hagen, I., ... Volgers, G. (2017). Een beeldend verslag over het ontstaan en de ontwikkeling van Windwerk.
- Entwistle, N., & Heritage, G. (2017). *An evaluation DEM accuracy acquired using a small unmanned aerial vehicle across a riverine environment Entwistle, NS and Heritage, G Title An evaluation DEM accuracy acquired using a small unmanned aerial vehicle across a riverine environment*.
- Gabler, R. E., Petersen, J. F., & Trapasso, L. M. (2006). *Essentials of Physical Geography*. Brooks Cole.
- Hesp, P. (2002). Fore-dunes and blowouts: initiation, geomorphology and dynamics. *Geomorphology*, 48(1–3), 245–268. [https://doi.org/10.1016/S0169-555X\(02\)00184-8](https://doi.org/10.1016/S0169-555X(02)00184-8)
- Jackson, D. W. T., Cooper, J. A. G., & Green, A. N. (2014). A preliminary classification of coastal sand dunes of KwaZulu-Natal. *Journal of Coastal Research*, 70(May), 718–722. <https://doi.org/10.2112/SI70-121.1>
- Keijsers, J. G. S., De Groot, A. V., & Riksen, M. J. P. M. (2015). Vegetation and sedimentation on coastal foredunes. *Geomorphology*, 228, 723–734. <https://doi.org/10.1016/j.geomorph.2014.10.027>
- Kidwell, D. M., Dietrich, J. C., Hagen, S. C., & Medeiros, S. C. (2016). Impacts of the coastal dynamics of

- sea level rise on low gradient coastal landscapes. *Earth's Future*, 5(1), 2–9. <https://doi.org/10.1002/2016EF000493>
- Koningsveld, M. V., Otten, C. J., & Mulder, J. P. M. (2007). DUNES: THE NETHERLANDS SOFT BUT SECURE SEA DEFENCES. In *westerndredging.org* (pp. 167–184). Retrieved from https://www.westerndredging.org/phocadownload/ConferencePresentations/2007_WODA_Florida/Session2B-BeneficialUsesofDredging/2 - van Koningsveld, et al - Dunes, The Netherland's Soft but Secure Sea Defences.pdf
- Luijendijk, A., Hagenaars, G., Ranasinghe, R., & Baart, F. (2018). The State of the World ' s Beaches. *Scientific Reports*. <https://doi.org/10.1038/s41598-018-24630-6>
- Lynch, K., Jackson, D. W. T. , & Cooper, j. A. G. (2016). The fetch effect on aeolian sediment transport on a sandy beach : a case study from Magilligan Strand , 1135(April), 1129–1135. <https://doi.org/10.1002/esp.3930>
- Mancini, F., Dubbini, M., Gattelli, M., Stecchi, F., Fabbri, S., & Gabbianelli, G. (2013). Using unmanned aerial vehicles (UAV) for high-resolution reconstruction of topography: The structure from motion approach on coastal environments. *Remote Sensing*, 5(12), 6880–6898. <https://doi.org/10.3390/rs5126880>
- Masek, J. G., Hayes, D. J., Joseph Hughes, M., Healey, S. P., & Turner, D. P. (2015). The role of remote sensing in process-scaling studies of managed forest ecosystems. *Forest Ecology and Management*, 355, 109–123. <https://doi.org/10.1016/j.foreco.2015.05.032>
- Maun, M. A. (2009). *The biology of coastal sand dunes*. Oxford University press (Vol. 104). <https://doi.org/10.1093/aob/mcp136>
- Montreuil, A. L., Bullard, J. E., Chandler, J. H., & Millett, J. (2013). Decadal and seasonal development of embryo dunes on an accreting macrotidal beach: North Lincolnshire, UK. *Earth Surface Processes and Landforms*, 38(15), 1851–1868. <https://doi.org/10.1002/esp.3432>
- Nolet, C., van Puijenbroek, M., Suomalainen, J., Limpens, J., & Riksen, M. (2017). UAV-imaging to model growth response of marram grass to sand burial: Implications for coastal dune development. *Aeolian Research*, (March), 0–1. <https://doi.org/10.1016/j.aeolia.2017.08.006>
- Peterson, Klein, & Stewart. (2015). *Whitepaper on Structure from Motion (SfM) Photogrammetry: Constructing Three Dimensional Models from Photography*.
- Reim, E. (2013). *Annual aeolian sediment transport from the intertidal beach*. UNIVERSITY OF TWENTE.
- Roggema. (2009). *Adaptation to Climate Change: A Spatial Challenge*. Springer Dordrecht Heidelberg London New York. <https://doi.org/10.1007/978-1-4020-9359-3>
- Rosenberg, P. (1955). Information theory and electronic photogrammetry. *Photogrammetric Engineering*, 21(4), 543–555.
- Saito, and S. W. P. P. I. J. L. J.-P. G. J. H. A. K. K. L. M. (2013). *Chapter 5: Coastal Systems and Low-Lying Areas. Climate Change 2014: Impacts, Adaptation, and Vulnerability. Part A: Global and Sectoral Aspects. Contribution of Working Group II to the Fifth Assessment Report of the Intergovernmental Panel on Climate Change*. Cambridge University Press. <https://doi.org/10.1017/CBO9781107415379.010>
- Sigren, J. M., Figlus, J., Armitage, A. R., Barone, D. A., McKenna, K. K., Farrell, S. C., ... Cohn, N. T. (2014). Coastal sand dunes and dune vegetation: restoration, erosion, and storm protection. *Shore & Beach*, 82(4), 5.
- Smith, M. W., Carrivick, J. L., & Quincey, D. J. (2015). Structure from motion photogrammetry in physical geography. *Progress in Physical Geography*. <https://doi.org/10.1177/0309133315615805>
- Suomalainen, J., Anders, N., Iqbal, S., Roerink, G., Franke, J., Wenting, P., ... Kooistra, L. (2014). A lightweight hyperspectral mapping system and photogrammetric processing chain for unmanned aerial vehicles. *Remote Sensing*. <https://doi.org/10.3390/rs6111013>
- Taddia, Y., Corbau, C., Zambello, E., Russo, V., Simeoni, U., Russo, P., ... Photoscan, A. (2016). UAVS TO ASSESS THE EVOLUTION OF EMBRYO DUNES.
- USGS. (2017). National Unmanned Aircraft Systems (UAS) Project Office Processing UAS Imagery using Agisoft Photoscan. DENVER, COLORADO: USGS National UAS Project Office. Retrieved from

- <https://uas.usgs.gov/pdf/BauerPhotoscanNASAMarch2017.pdf>
- van Puijenbroek, M., Limpens, J., de Groot, A. V., Riksen, M. J. P. M., Gleichman, M., Slim, P. A., ... Berendse, F. (2017). Embryo dune development drivers: beach morphology, growing season precipitation, and storms. *Earth Surface Processes and Landforms*, 42(11), 1733–1744. <https://doi.org/10.1002/esp.4144>
- van Puijenbroek, M., Nolet, C., Groot, D., Suomalainen, Riksen, Berendse, & Limpens. (2017). Exploring the contributions of vegetation and dune size to early dune building using unmanned aerial vehicle (UAV)-imaging. *Biogeosciences Discussions*, 170, 1–44. <https://doi.org/10.5194/bg-2017-170>
- Verhagen, H. J. (1990). Coastal Protection and Dune Management in The Netherlands. *J. of Coastal Research*, 6(1), 169–179.
- Vosselman, G. (2000). Slope based filtering of laser altimetry data. *International Archives of Photogrammetry and Remote Sensing*, Vol. 33, Part B3/2, 33(Part B3/2), 678–684. [https://doi.org/10.1016/S0924-2716\(98\)00009-4](https://doi.org/10.1016/S0924-2716(98)00009-4)
- Wang, M. (2014). Spatio-temporal variability in accretion and erosion of coastal foredunes in the Netherlands: Regional climate and local topography. *PLoS ONE*, 9(3). <https://doi.org/10.1371/journal.pone.0091115>
- Yandong Wang, M. M. (2001). AUTOMATIC DETECTION OF SHADOW POINTS IN DIGITAL IMAGES FOR AUTOMATIC TRIANGULATION.
- Yang, W., Wang, S., Zhao, X., Zhang, J., & Feng, J. (2015). Greenness identification based on HSV decision tree. *Information Processing in Agriculture*. <https://doi.org/10.1016/j.inpa.2015.07.003>

Appendices

Appendix A - Weather conditions around campaigns

Appendix B - Used settings in Agisoft Photoscan Pro

Appendix C - Digital Surface Models

Appendix D - Cross sections DSM

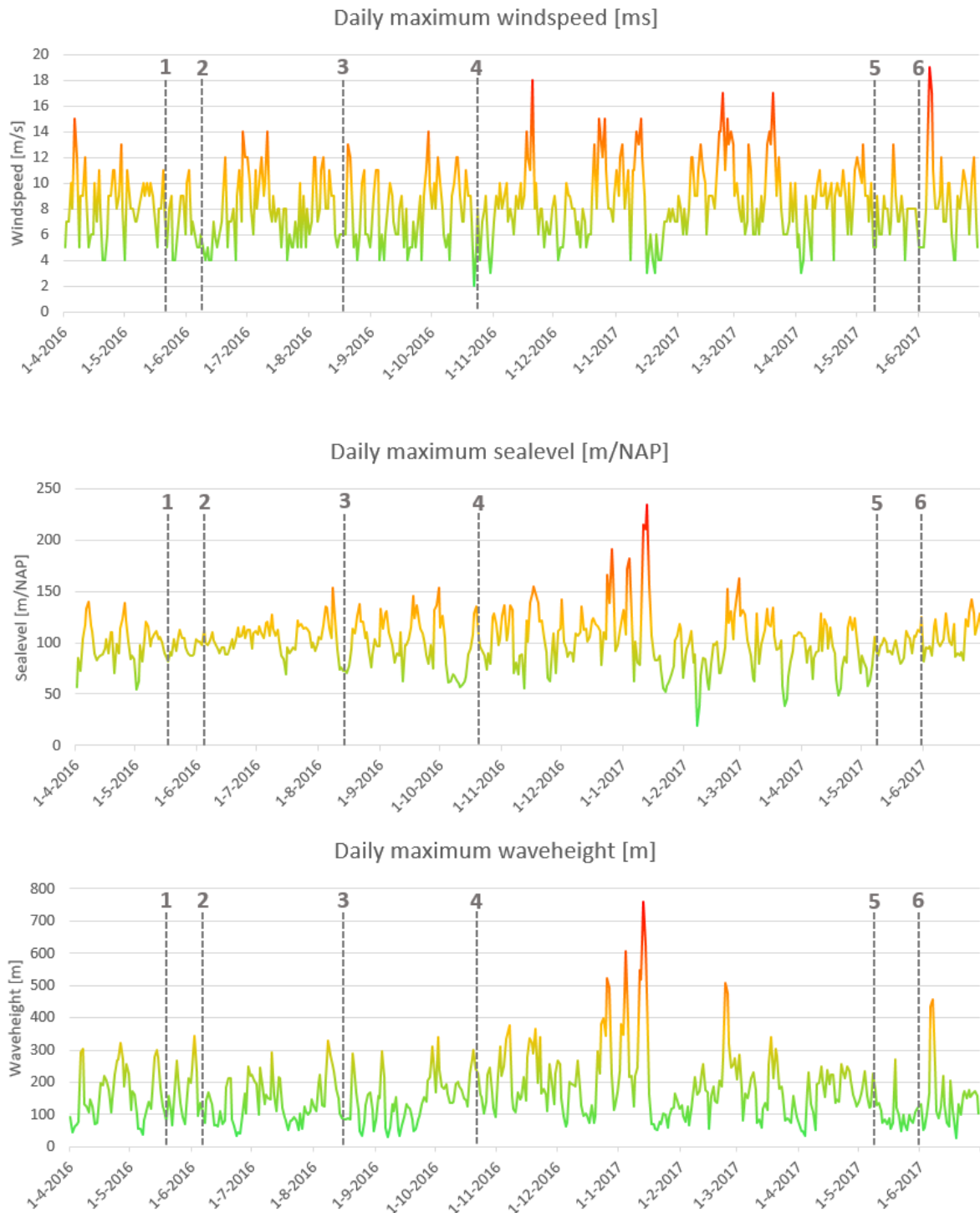
Appendix E – Dune height models

Appendix F – Overview individual studied fields

Appendix G– Used SAGA GIS tools and software settings

Appendix A - Weather conditions around campaigns

Hoorn (Terschelling) and buoy nearby. From KNMI daily maximum data. The numbers in the graphs represent the UAV acquisition campaigns; (1) May 2016, (2) June 2016, (3) August 2016, (4) November 2016, (5) May 2017, (6) June 2017.



Appendix B - Used settings in Agisoft Photoscan Pro 1.4

The following Agisoft Photoscan workflow and its settings were applied to all six datasets of this study containing ENDVI imagery.

Step 1: Align Photos

- Accuracy: Medium
- Generic preselection checked
- Key point limit: 40000 (default)
- Tie point limit: 0 (no limit)
- Adaptive camera model fitting checked

Step 2: Add coordinates of ground control points to Agisoft

A text file containing all exact coordinates of the referencing points (referencing poles and beach poles) was used to reference all six models. These coordinates were accurately measured using an RTK (base + rover) system.

- Add the GCP file to Agisoft using the “import” option within the Reference pane
- Set the coordinate system within the reference setting to Amersfoort / RD New (EPSG:28992)
- Find a photo containing a ground control point
- Open the photo by double clicking, zoom in to the middle of the control point, right-click the centre location and select “Place Marker” to select the corresponding marker/control point
- Right-click the marker and select “Filter by Marker”. Agisoft will find matching images and will estimate the GCP marker. Adjust (if necessary) all estimated markers for all matching images. The blue flag will now change to green
- Repeat the steps above for the next GCP’s
- Click update 

Step 3: (Camera) calibration

- Go to “Camera calibration” within the Tools-tab
- Camera type: Frame
- For the first dataset: Go to the “Adjusted” tab and export the camera parameters which were calculated by Agisoft 
- For all other datasets: Go to the “Adjusted” tab and import the Agisoft Camera Calibration file (*.xml). This is done to handle all datasets equally and use the same camera parameters. This can only be done if the same sensor setup is used.
- Go to “Optimize Camera Alignment” and select all checkboxes. This will optimize for camera distortion and improve the result 

Step 4: Check the errors of the markers

In the reference pane, check the total error in meters for all markers. If the error is relatively high (e.g. >0.3m for this study), double check if all markers are placed correctly. Redo the allignment with higher accuracy settings or alternatively uncheck the marker to decrease the overall error.

Step 5: Optimize Alignment

- Use default settings

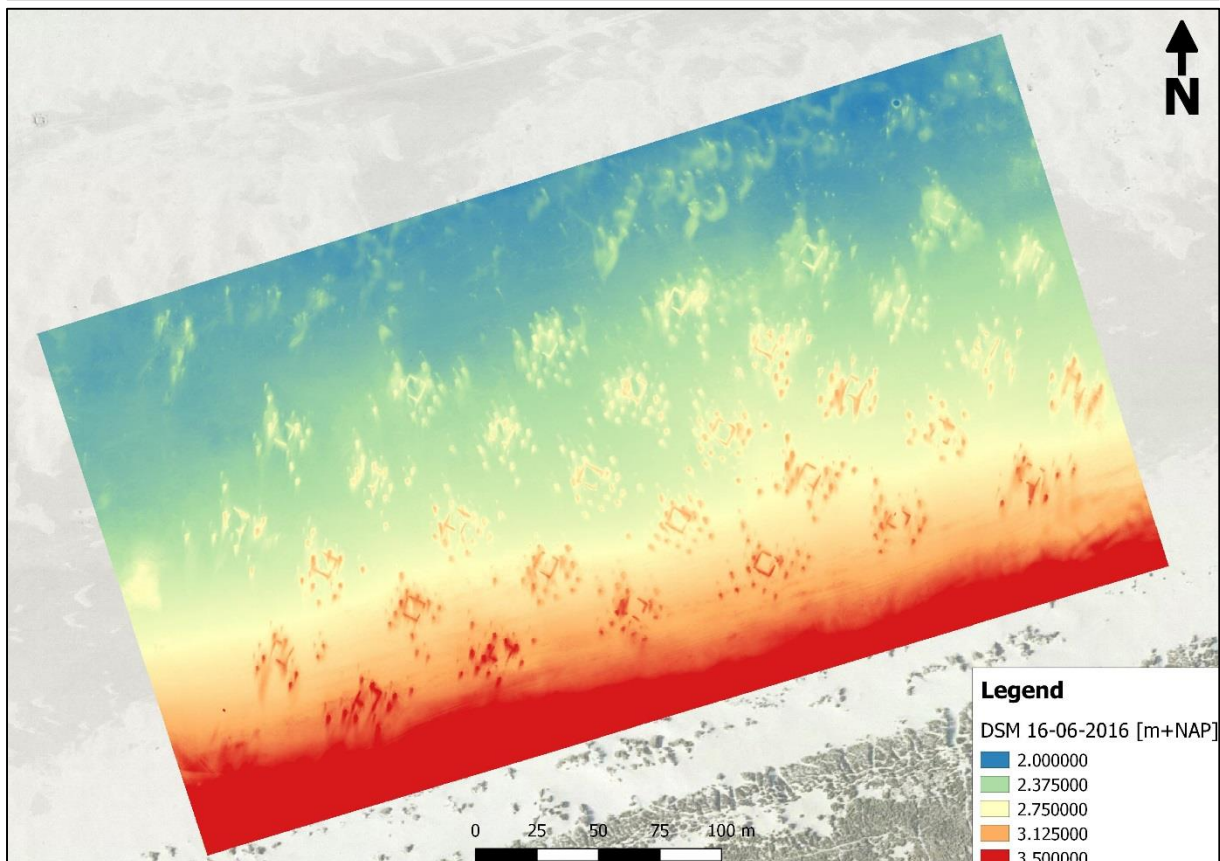
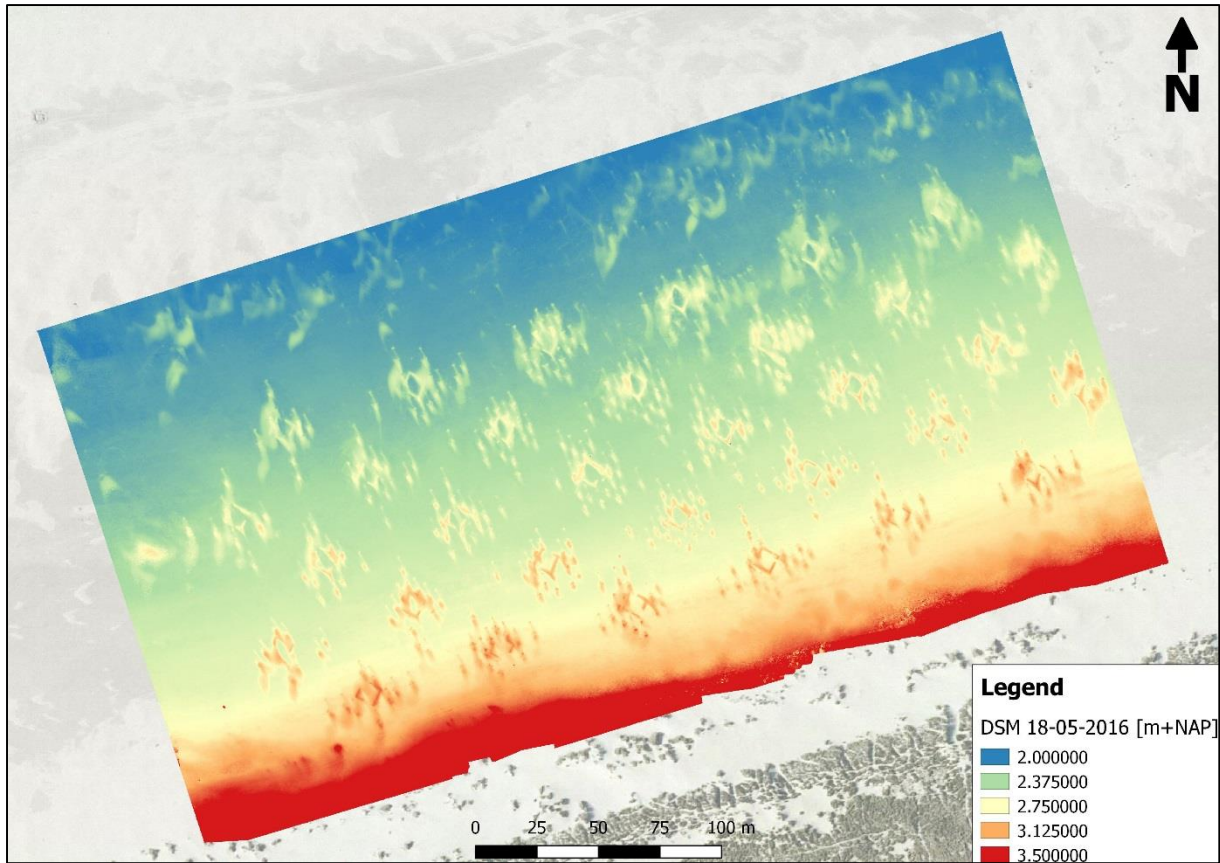
Step 6: Batch process Agisoft steps

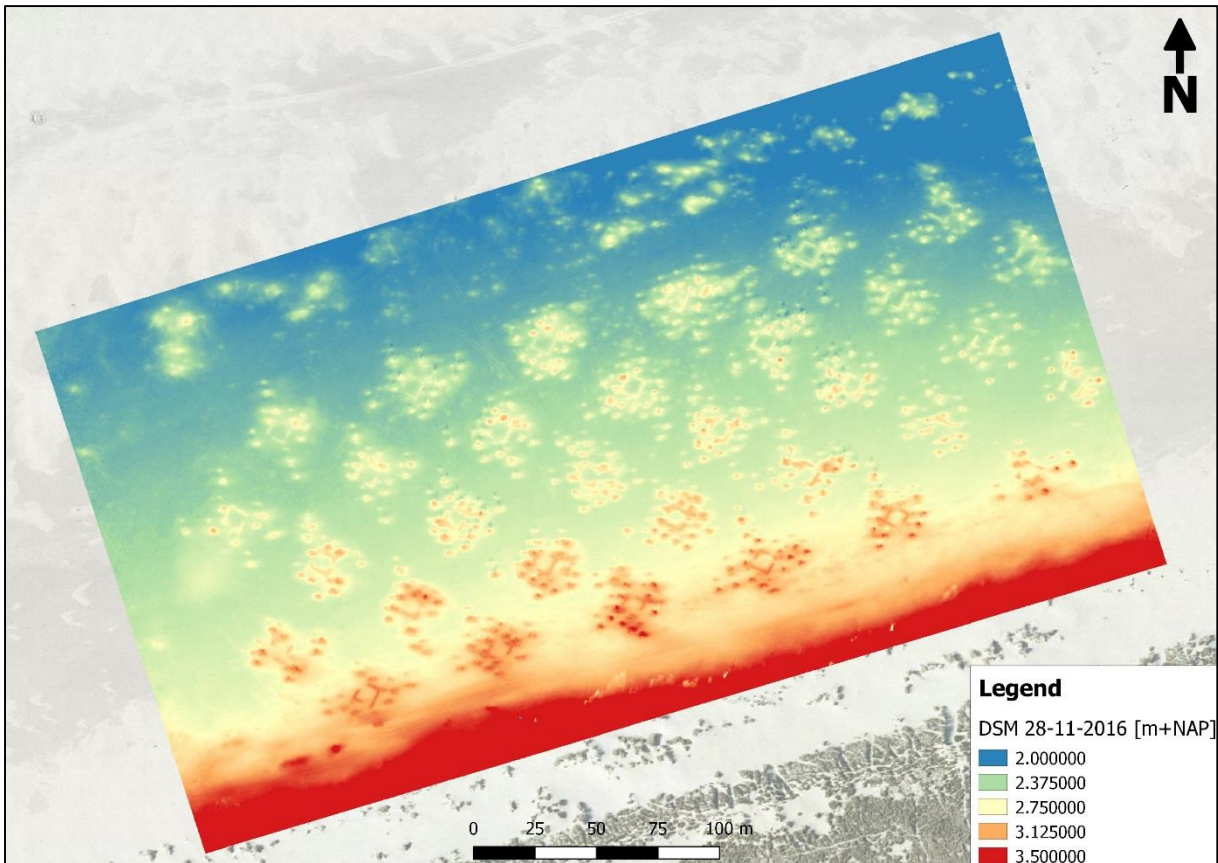
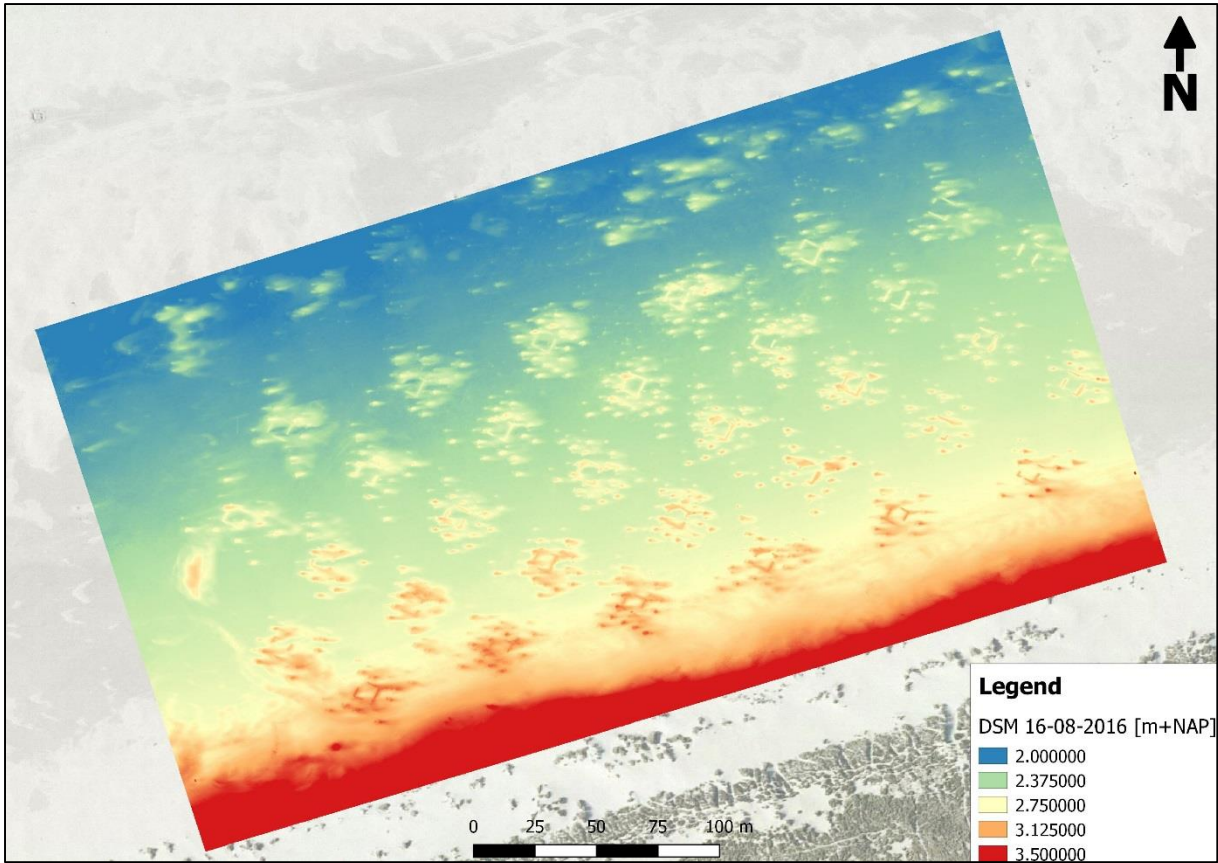
The following Agisoft steps were batch processed because they can be quite time consuming (1-2 processing days). To do so, click the "Workflow" tab and select "Batch Process...". Add a new job for the following processing steps:

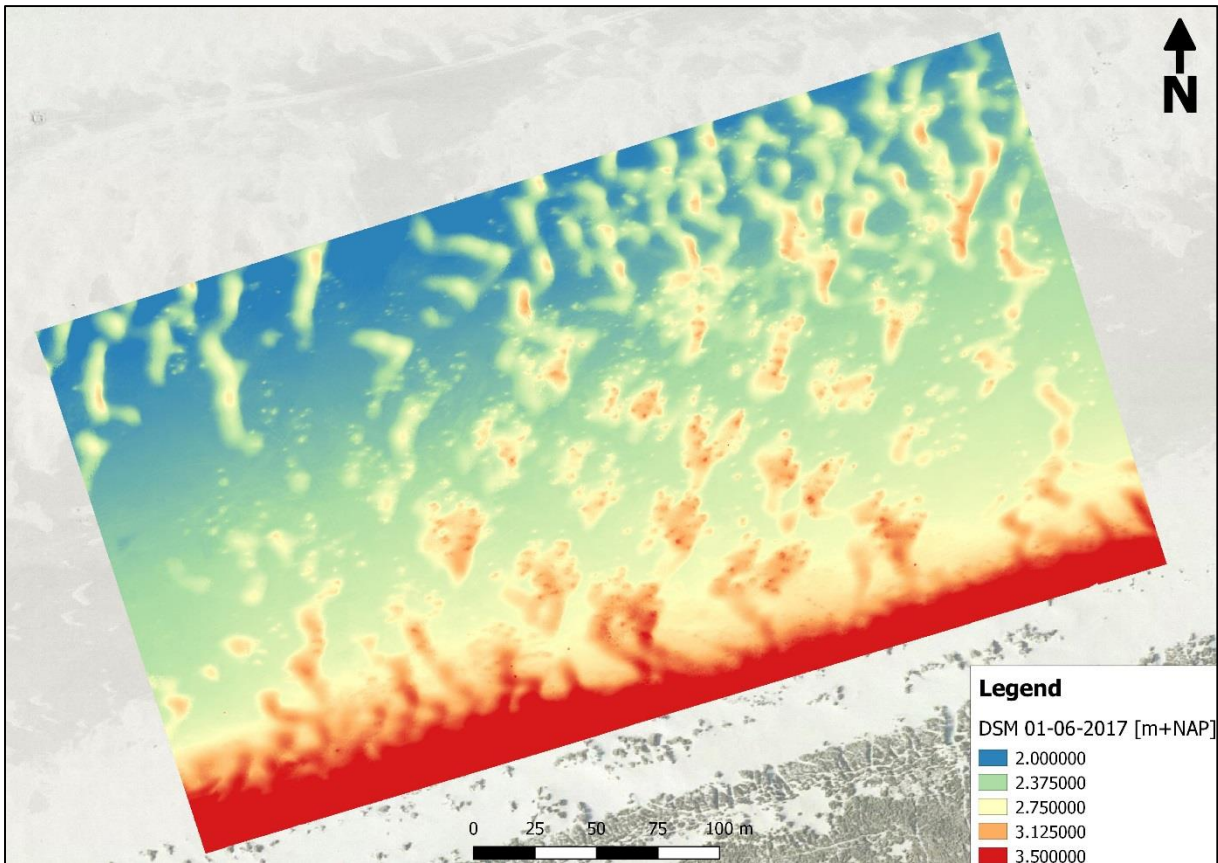
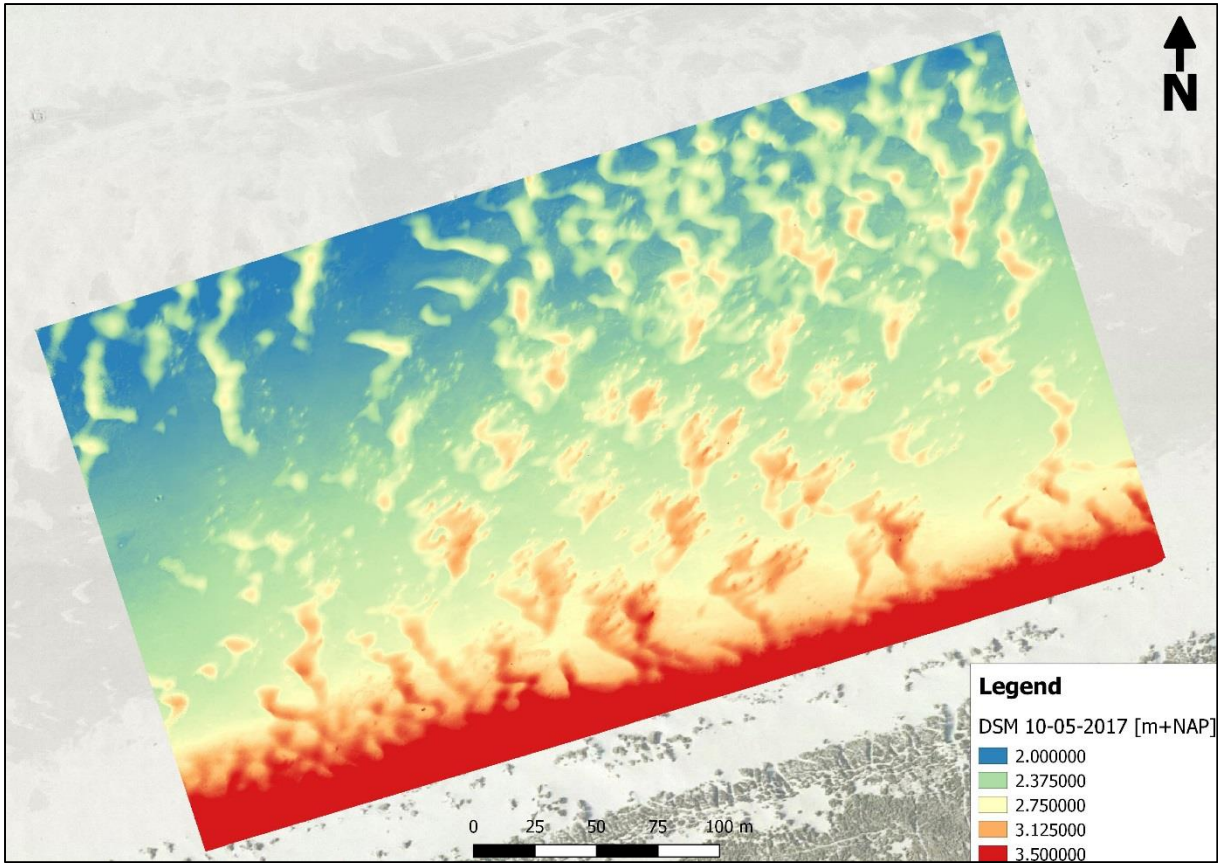
- i. Build Dense Cloud**
 - Quality: Medium
 - Depth filtering: Aggressive
 - Reuse depth maps: No
 - Calculate point colors: Yes
- ii. Build Mesh**
 - Surface type: Height field
 - Source data: Dense cloud
 - Face count: Custom
 - Custom face count: 99999999999
 - Interpolation: Enabled (default)
 - Point classes: All
 - Calculate vertex colors: Yes
- iii. Build texture**
 - Mapping mode: Adaptive orthophoto
 - Blending mode: Mosaic
 - Texture size: 4096
 - Texture count: 1
 - Hole filling: Yes
- iv. Build DEM**
 - Projection: Amersfoort / RD New
 - Source data: Dense cloud
 - Interpolation: Enabled
 - Point classes: All
 - Resolution: 0.05 m
 - Total size: automatically calculated (do not change)
- v. Build orthomosaic**
 - Projection: Amersfoort / RD New
 - Surface: DEM
 - Blending mode: Average
 - Pixel size: 0.1 m
- vi. Export DEM**
 - ...
- vii. Export Orthophoto**
 - ...

Appendix C - Digital Surface Models

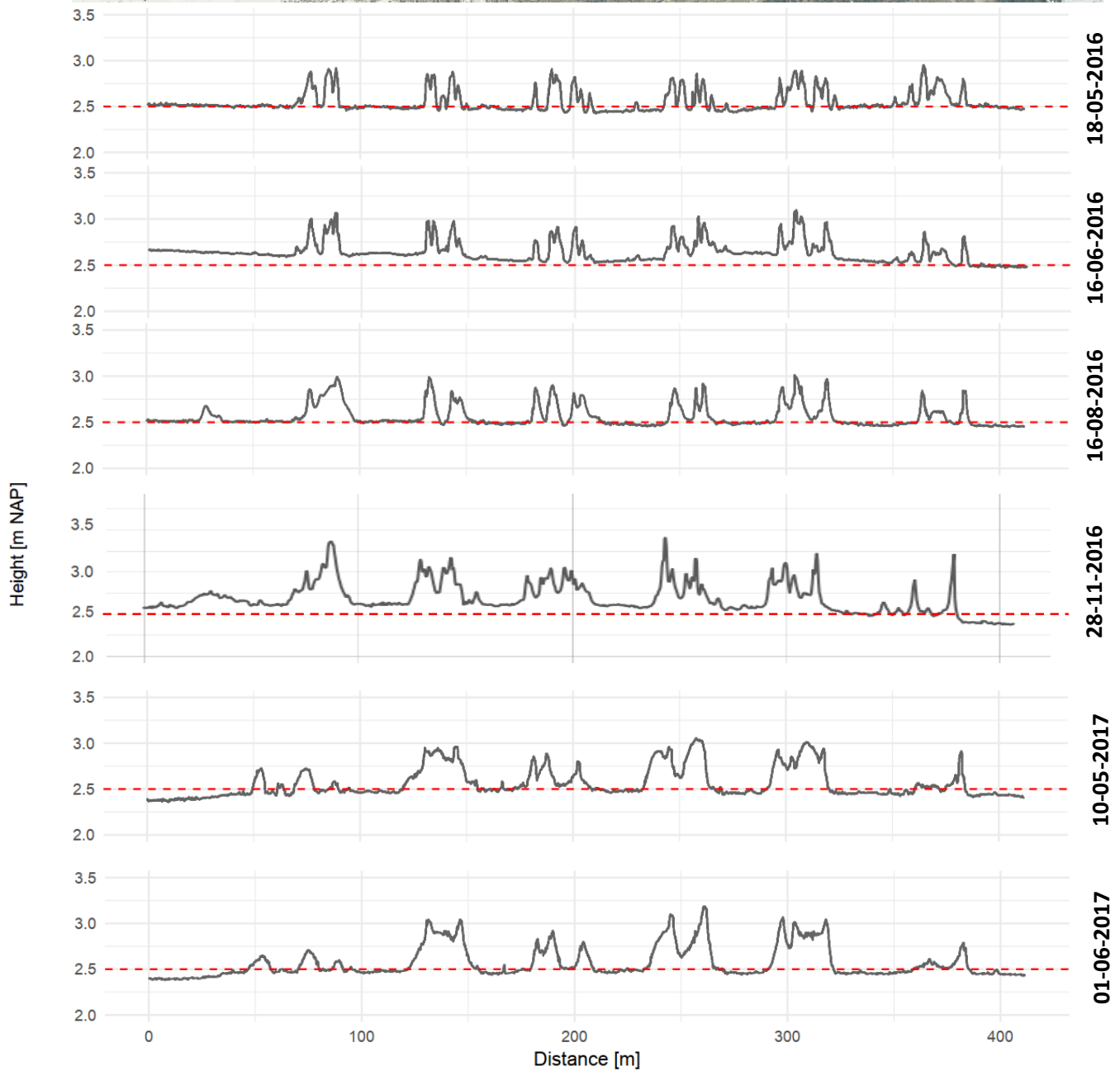
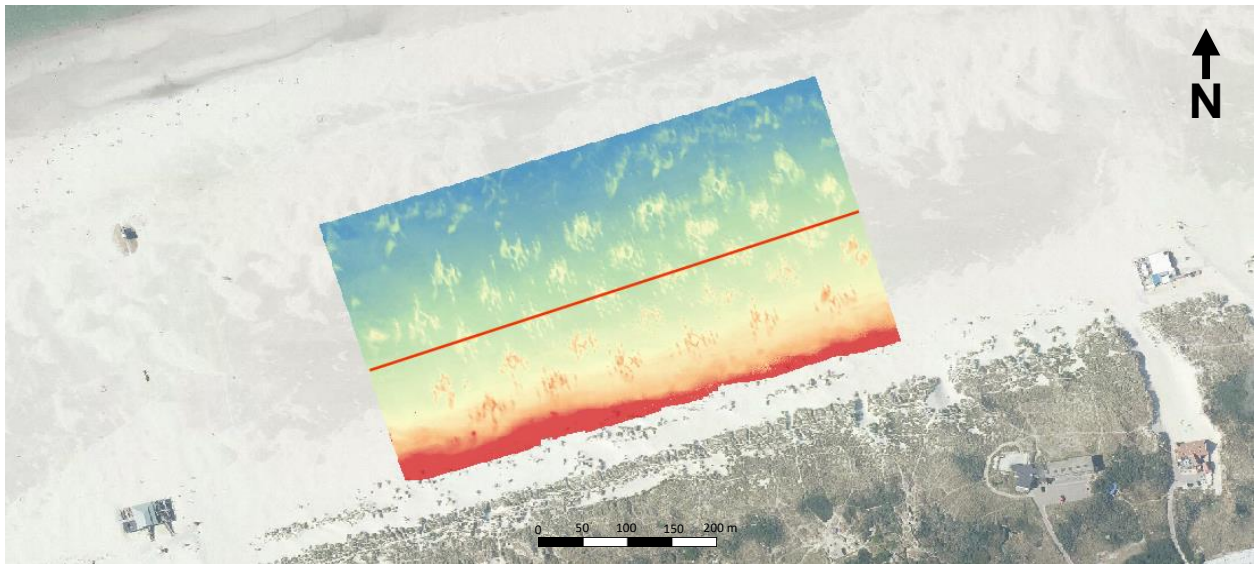
Digital surface models which were created in Agisoft Photoscan Pro:



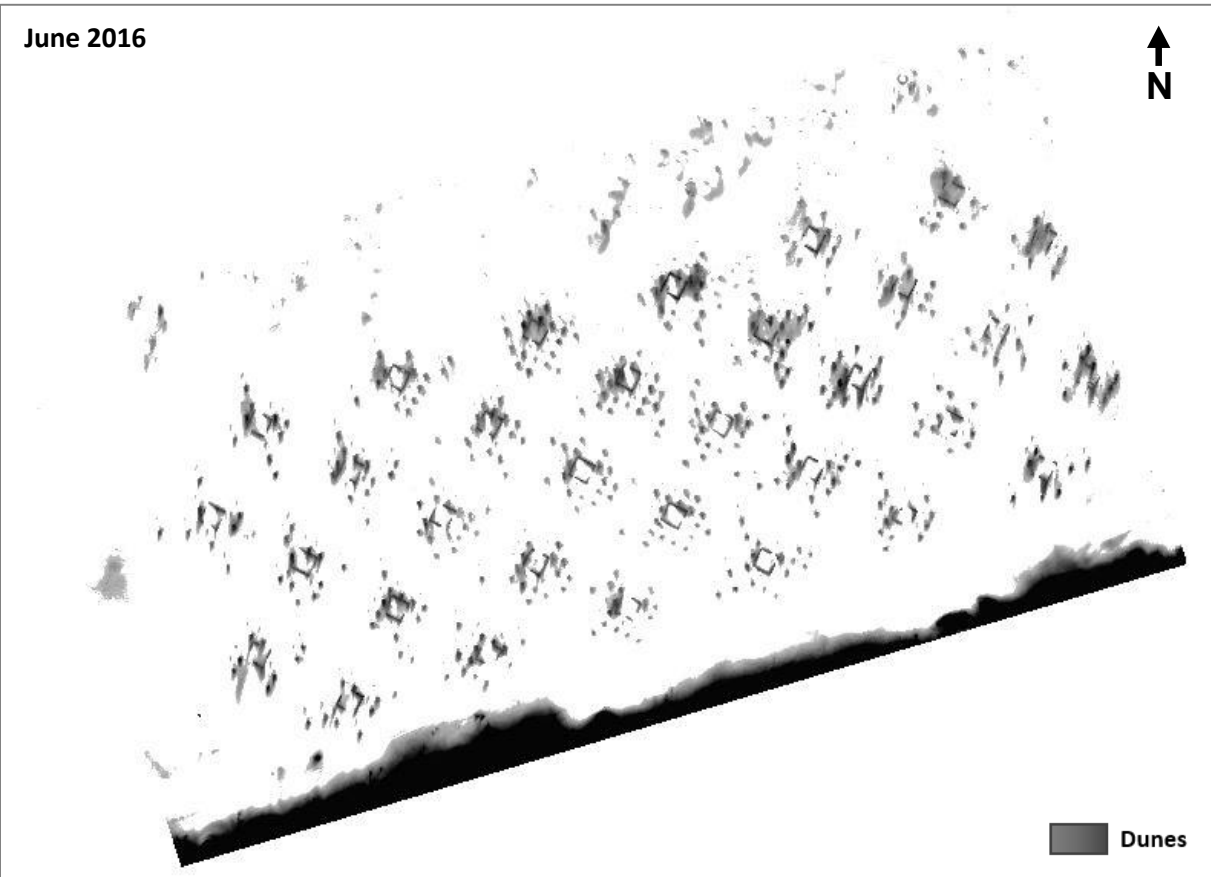
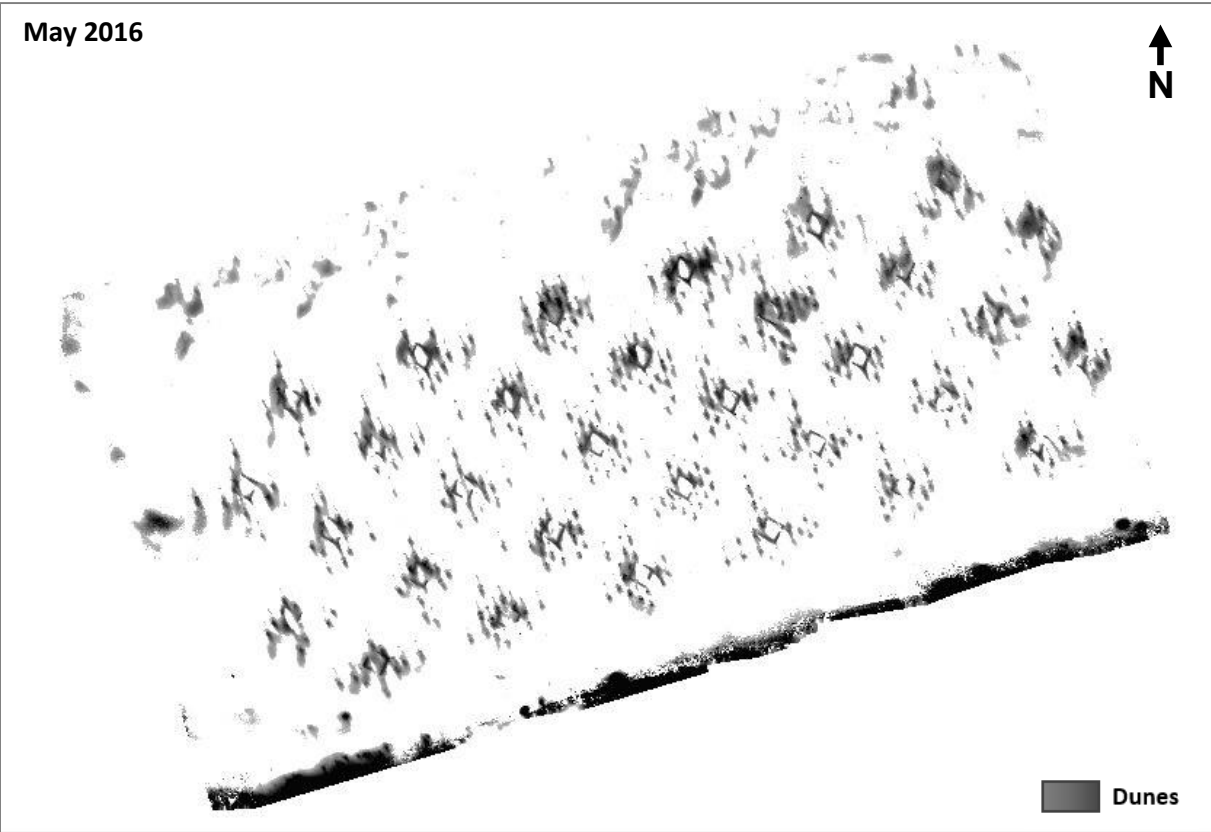




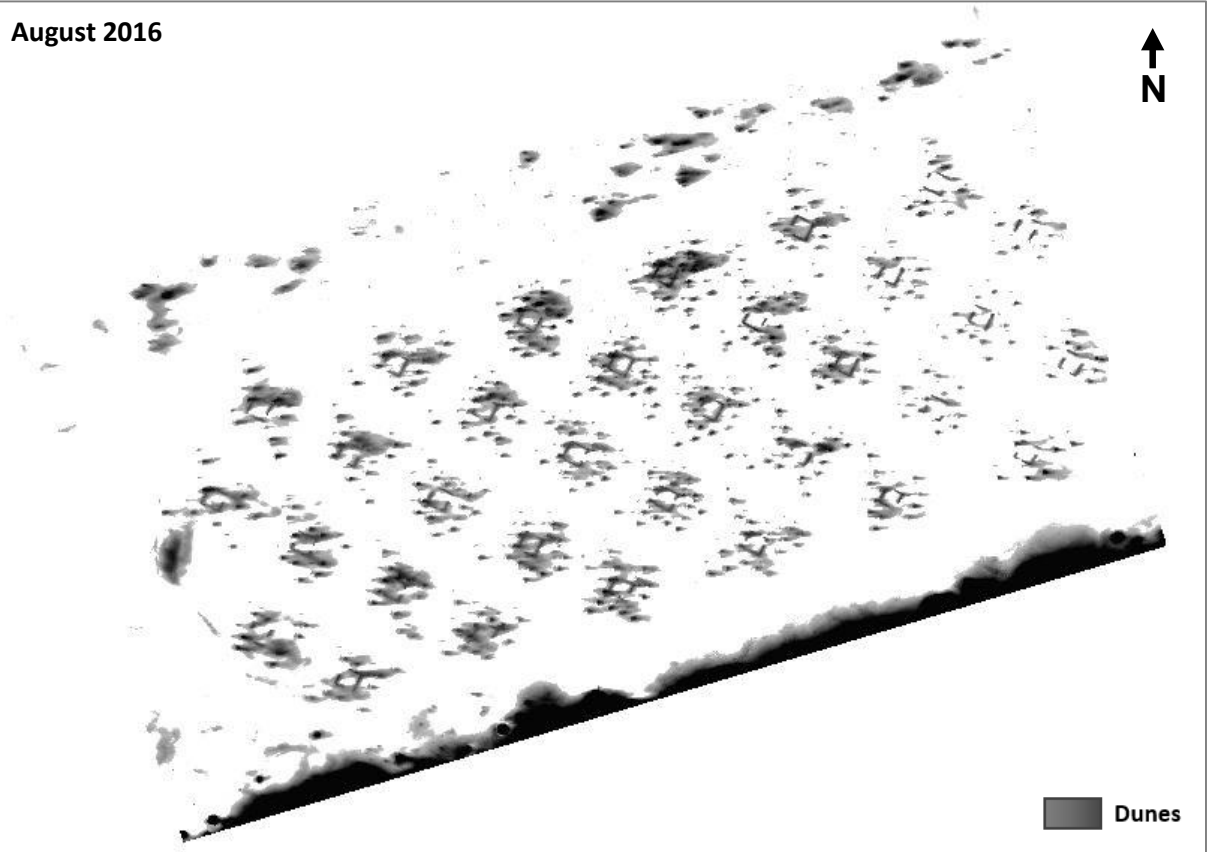
Appendix D - Cross sections DSM



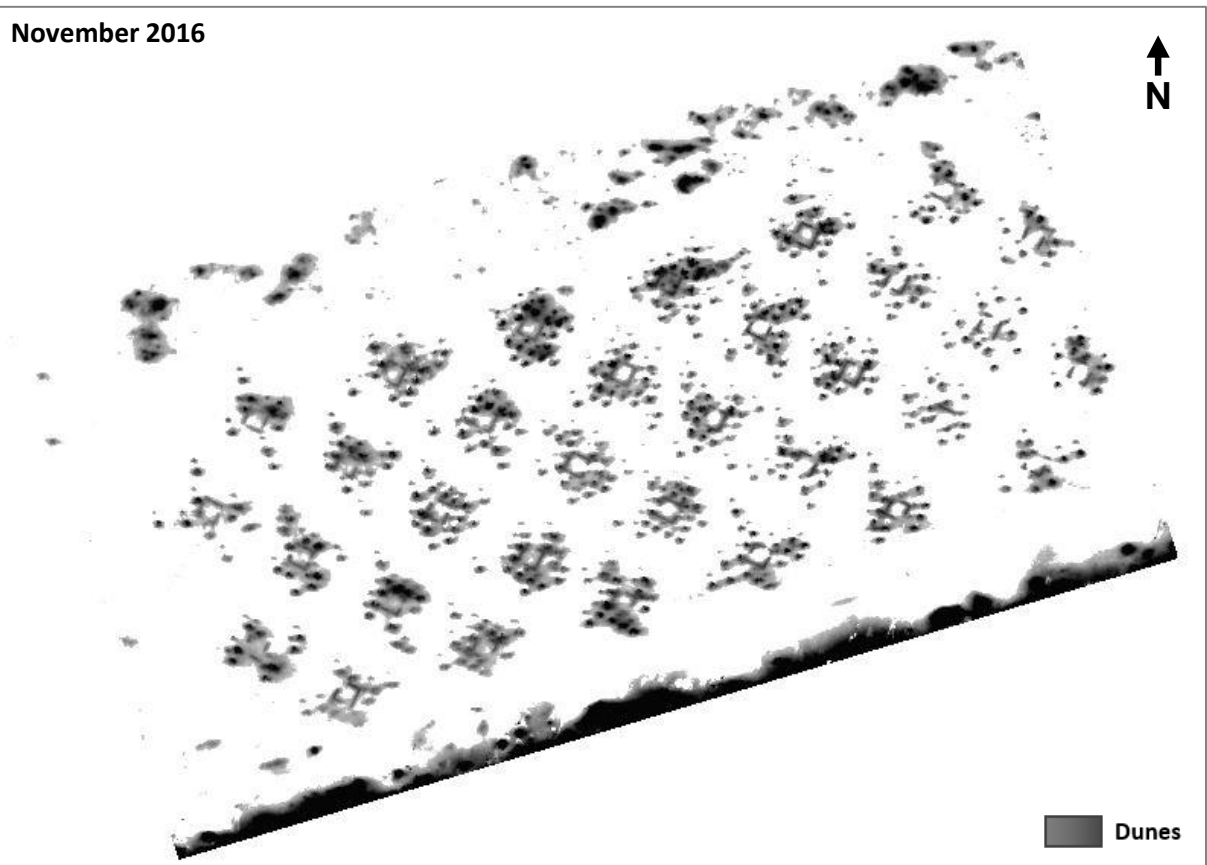
Appendix E – Dune height models



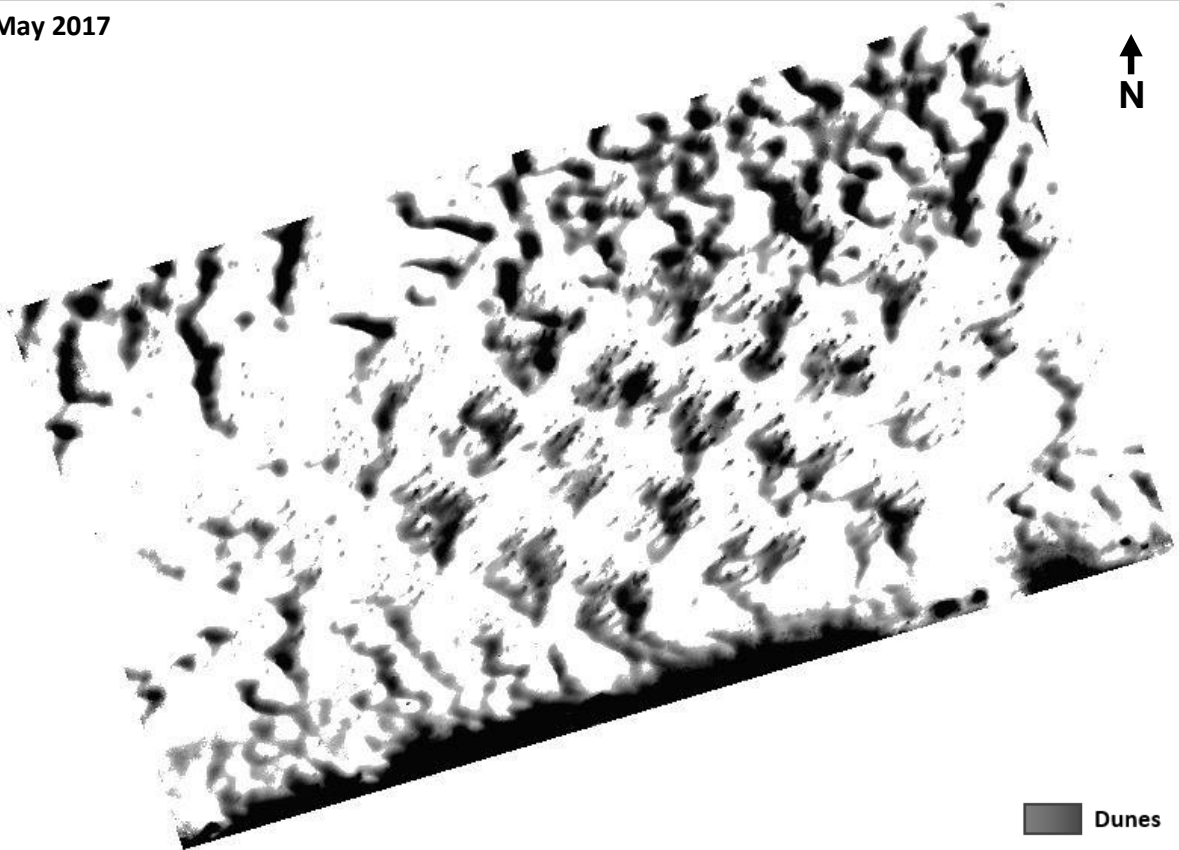
August 2016



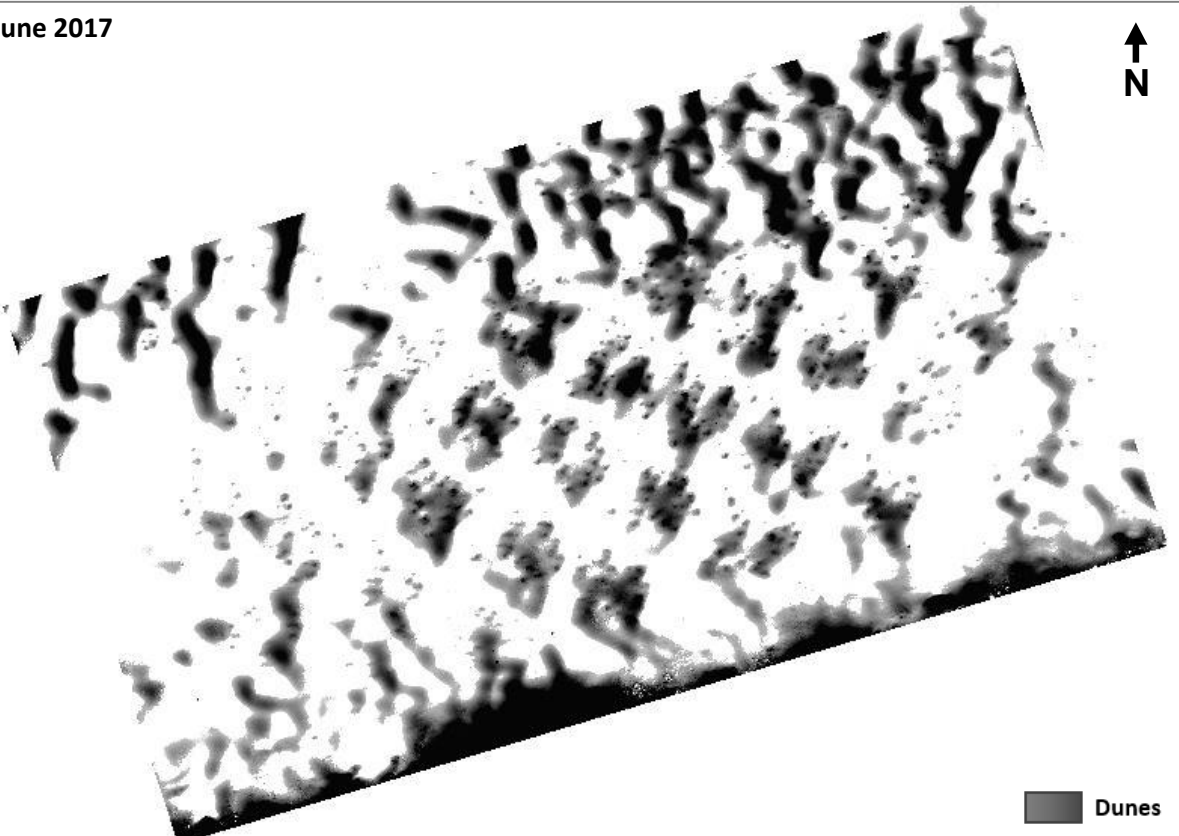
November 2016



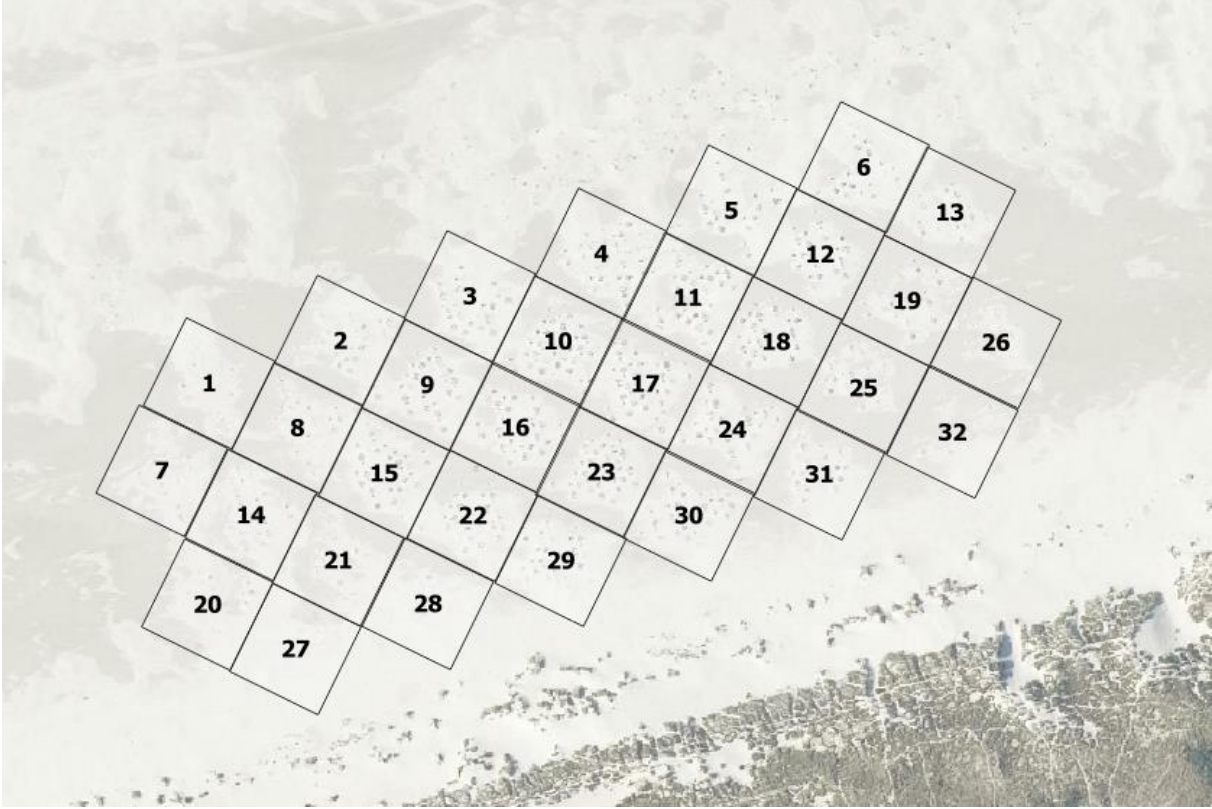
May 2017



June 2017



Appendix F – Overview individual studied fields



Appendix G – Used SAGA GIS tools and software settings

Interpolation of vegetation:

Close Gaps with Spline

Data Objects	
Grids	
Grid system	<no choice available>
>> Grid	<not set>
> Mask	<not set>
< Closed Gaps Grid	<not set>
Options	
Only Process Gaps with Less Cells	0
Maximum Points	1000
Number of Points for Local Interpolation	10
Extended Neighbourhood	<input checked="" type="checkbox"/>
Neighbourhood	Neumann
Radius (Cells)	8
Relaxation	0

Grid system
Grid system
Grid system

Buttons: Okay, Cancel, Load, Save, Defaults

Slope-based filter for DHM extraction:

DTM Filter (slope-based)

Data Objects	
Grids	
Grid system	<no choice available>
>> Grid to filter	<not set>
<< Bare Earth	<create>
<< Removed Objects	<create>
Options	
Search Radius	1
Approx. Terrain Slope	2
Use Confidence Interval	<input type="checkbox"/>

Data Objects

Buttons: Okay, Cancel, Load, Save, Defaults

Interpolating beach base plane:

Multilevel B-Spline Interpolation (from Grid) ✕

Data Objects	
Grids	
Grid system	<no choice available>
>> Grid	<not set>
Options	
Target Grid System	grid or grid system
Grid System	<no choice available>
<< Target Grid	<create>
Method	with B-spline refinement
Threshold Error	0.0001
Maximum Level	4
Update View	<input type="checkbox"/>
Data Type	floating point

Maximum Level
Integer
Minimum: 1
Maximum: 14
Default: 11

Okay
Cancel
Load
Save
Defaults